ISSN 2167-1273
Volume 2, Issue11, November 2013

FEA Information Engineering Journal

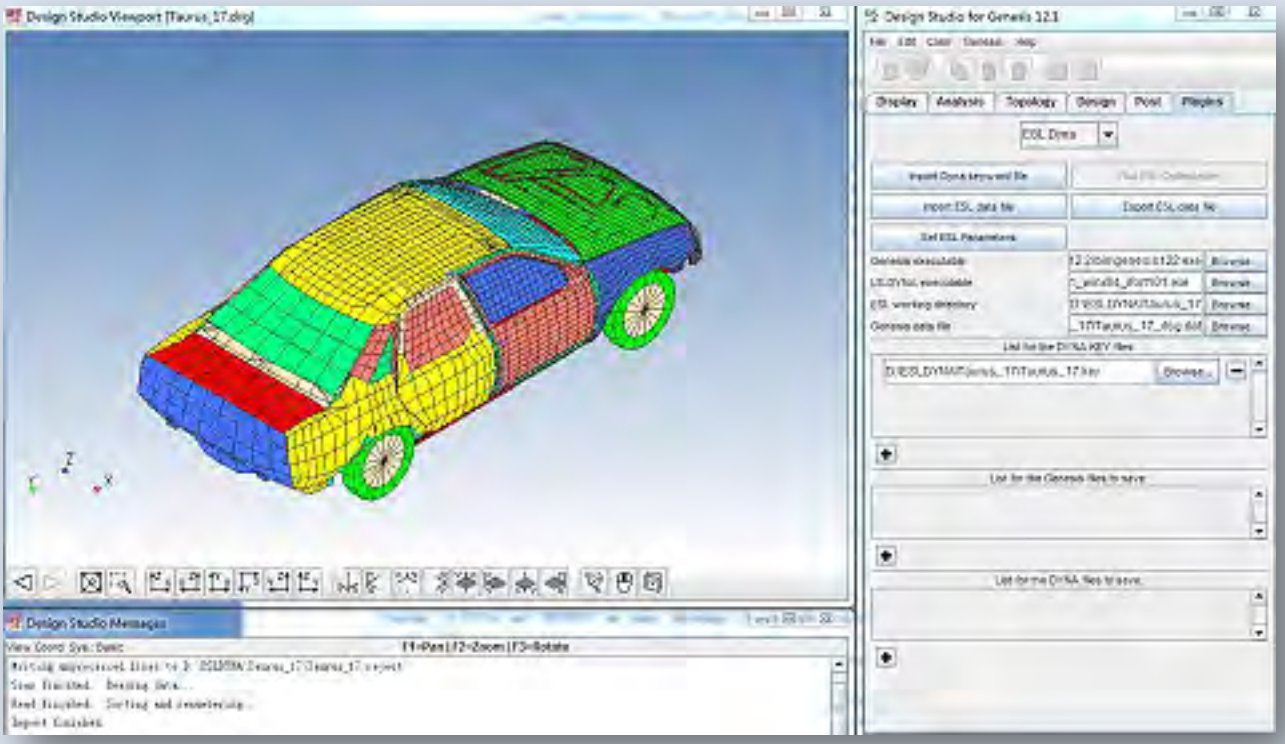

第一届中国 LS-DYNA 用户大会文集

1st China LS-DYNA® Users Conference

Aim and Scope

FEA Information Engineering Journal (FEAIEJ™) is a monthly published online journal to cover the latest Finite Element Analysis Technologies. The journal aims to cover previous noteworthy published papers and original papers. All published papers are peer reviewed in the respective FEA engineering fields.

Consideration is given to all aspects of technically excellent written information without limitation on length. All submissions must follow guidelines for publishing a paper, or periodical. If a paper has been previously published, FEAIEJ requires written permission to reprint, with the proper acknowledgement give to the publisher of the published work.

 FEAIJ welcomes unsolicited topics, ideas, and articles.

Monthly publication is limited to no more then five papers, either reprint, or original. Papers will be archived on www.feaiej.com

For information on publishing a paper original or reprint contact editor@feaiej.com Subject line: Journal Publication

Cover: Figure 3 combine LS-DYNA analysis and GENESIS optimization

Nonlinear Crashworthiness Optimization integrated with LS-DYNA and Equivalent Static Load method

FEA Information Engineering Journal

TABLE OF CONTENTS

Volume 2, Issue No. 11 November 2013

Parameter research of vehicle crash test dummy skin material

Hua Xin , Yan Lingbo, Zhang Guanjun, Zhang Kai

(State Key Laboratory of Advanced Design and Manufacturing for Vehicle Body, Changsha, 410082)

Abstract: According to the characteristics of dummy skin, a series of uniaxial compression tests are conducted (strain rates of $0.01s^{-1}$, $0.1s^{-1}$, $1s^{-1}$ and engineer strain levels of 10%, 20% and 30%) and parameters of two-term OGDEN model are obtained by fitting the test data. Finite element simulation model of test is build and a group of optimal parameters which allowed the minimum error between the data of test and simulation is acquired by optimizing the four material parameters of two-term OGDEN model with Hybrid genetic algorithm.

Key words: Dummy skin; OGDEN model; Hybrid genetic algorithm; Reverse technology

0 Introduction

Vehicle crash test dummy is indispensable equipment used in tests with great risk and uncertain for human. The skin material as mainly biomimetic material of vehicle crash test dummy belongs to the polymer of polyvinyl chloride, whose solidity decides the position of skin on dummy. All kind of dummy skin is produced by polyvinyl chloride with solidity between shore A 40 and shore A 50. Dummy skin as biomimetic material is the first defense line of vehicle crash test dummy whose test result depends partly on the material properties of skin. [1,2] Research literature based on the parameter of dummy skin is limited and the value of parameters in simulation are difficult to accurately set. Accordingly, further study on parameters of dummy biomimetic material helps to improve the accuracy of dummy simulation analyst.

Xie Chi, Cai Peng etc. researched the structure of biomimetic material of vehicle crash test dummy by impact test, whose result show the feasibility of comprehensive assessment of the mechanical properties and impact strength of equivalence for the material.[3] However, the specific material parameters is not acquired. Sai S. Sarva, Stephanie Deschanel etc. compared the result of uniaxial tensile and uniaxial compression test from low to high strain rate for a polyurea and a polyurethane.[4] The results show great agreement in both uniaxial tensile and uniaxial compression test from slow and high strain rate, which provide a certain basis for selecting the test for dummy skin. Garrett W. Wood，Matthew B. Panzer etc. conducted uniaxial compression test for head skin of hybridⅢ dummy and compared four material models with finite element simulation.[5] The results show that two-term OGDEN model is the most suitable material model for hybridⅢ head skin in

finite element simulation, however, the test samples are acquired from assisted dummy head skin whose thickness is thin and the consistency of the sample thickness is hard to obtained.

Various sizes of sample are able obtained because the team are making vehicle crash test dummy. Tests and simulation research for dummy skin with solidity shore A 40 are conducted and parameters of dummy skin material are obtained by reverse research based on the former research.

1 Test

Viscoelastic material testing of rubbers may be performed using tension, compression and shear loading. Uniaxial tensile and uniaxial compression test are the most common test. [6-8] Uniaxial compression test are conducted considering compression is the most common load for vehicle crash test dummy skin. According to rubber physical test standard ISO8013-2006[9], the shape of sample is cylindrical. Four samples are obtained by dummy skin raw materials and the cylindrical mold with average diameter 29.5mm±0.5mm and average height 29.0mm±0.6mm. samples are placed in the standard room temperature (23℃±2℃) for 24 hours before test. Two end faces of samples are grinded in 12 hours before test to ensure the smoothness of the test samples. Lubrication for the two ends of the sample surface is conducted to reduce the effect of friction on the test results. In order to eliminate the gap between the pressure plate and the sample and reduce the error of test, 1N preload is used before loading.

The model of test device is INSTRON 5985 as shown in figure 1. Two kinds of test (strain rates of 0.01s-1, 0.1s-1, 1s-1 and engineer strain levels of 10%, 20% and 30%) are conducted to research the property of strain rate and relaxation. Information of compression force, displacement and time is recorded during the test. Engineer stress-strain curves of vehicle crash test dummy skin in three different strain rates under standard room temperature are in figure 2 and three different compression rates are in figure 3. Figure 4 shows four samples' engineer stress-strain curves under strain rate $20s^{-1}$ and compression rate 30%.

Figure 1 Test device INSTRON 5985

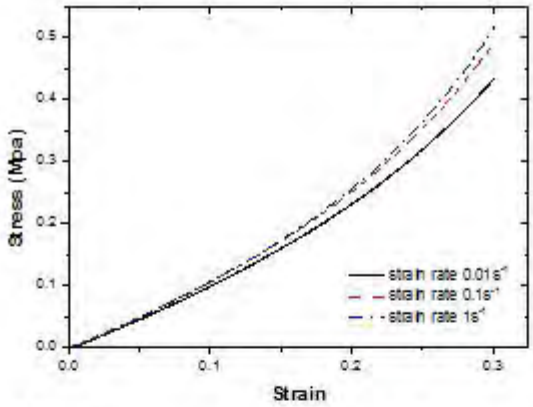

Figure 2 Engineer stress-strain curve in different strain rates

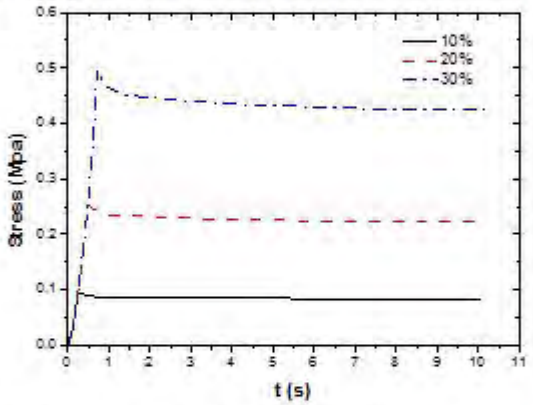

Figure 3 Engineer stress-strain curve in different compression rates

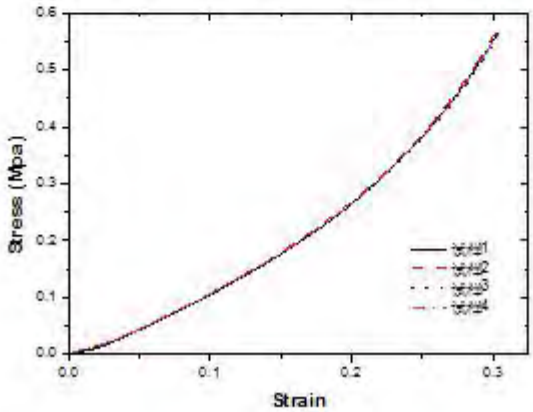

Figure 4 Engineer stress-strain curves of different samples

Curves in figure 2 shows the results in different strain rate are close. The maximum engineer stress between strain rate $0.01s^{-1}$and $0.1s^{-1}$(about 0.058Mpa) is 2.32 times than strain rate 0.1 s^{-1} and 1 s^{-1} (about 0.025Mpa). Curves in figure3 shows the results in different compression rate have great difference. The maximum engineer stress between compression rate 20% and 30% (about 0.19Mpa) is 1.36 times than compression rate 10% and 20% (about 0.14Mpa). Figure4 shows the results of four different samples is in great agreement, therefore, one of them is selected for the simulation analysis.

2 Simulation Analysis

2.1 OGDEN model

At present, the commonly used finite element analysis software which can describe skin viscoelastic constitutive models are Ogden model, Arruda Boyce model, Neo-Hookean model and the Mooney Rivlin model, etc. [10,11]。These models belong to the super-elastic model，basing on assumptions of super-elastic material volume nearly incompressible and isotropic. Usually hyper elastic materials is characterized by strain energy density function. Different constitutive models have different strain energy density function formula. Strain energy density function is a scalar function of strain or deformation tensor. The derivative of strain component is corresponding stress component。OGDEN model is a nonlinear hyper elastic model, which is widely used in engineer as it is simple in form, clear physical interpretation and wide applicable range. Its constitutive theory is that the strain energy density is three main independent function of elongation. The strain energy density function is showed as formula (1)，Where i is the order, λ_1, λ_2 and λ_3 for the three main elongation, μ_i and α_i for characterizing elastic parameters of materials.

$$W(\lambda_i) = \sum_i \frac{\mu_i}{\alpha_i}(\lambda_1^{\alpha_i} + \lambda_2^{\alpha_i} + \lambda_3^{\alpha_i} - 3) \quad (1)$$

Stress expression (2) is a convolution function, where stress is engineer stress. Expression is showed in the formula (3)。λ is elongation, showed in expression(4).

$$\sigma(\lambda, t) = \int_0^t g(t-\tau)\frac{d\varepsilon}{d\lambda}\frac{d\lambda}{d\tau}d\tau \quad (2)$$

$$\sigma = \frac{F}{A} = \lambda\frac{F}{A_0} \quad (3)$$

$$\lambda = \frac{l_0 + \Delta l}{l_0} \quad (4)$$

$g(t-\tau)$ in Formula (2) is the stress relaxation function, which is representation of the influence on dynamic yield stress bystrain rate during the deformation process. t is time，τ is the integration variable。Stress relaxation function is based on a series of Maxwell unit, as showed in formula (5-6).

$$g(t) = \alpha_0 + \sum_{i=1}^{N}\alpha_i e^{-\beta t} \quad (5)$$

$$g(t) = \sum_{i=1}^{n} G_i e^{-\beta_i t} \quad (6)$$

Formula (5) and (6) have the same meaning, which is the stress relaxation curve of different forms. This paper selected second OGDEN model to simulation dummy skin, ie the value of i takes 2。Then the stress of the uniaxial compression test is showed in expression (7), where μ_1, μ_2, α_1, α_2 representate the four the material properties parameters of dummy skin.

$$\sigma_{two} = \mu_1\left(\lambda^{\alpha_1} - \lambda^{-\frac{\alpha_1}{2}}\right) + \mu_2\left(\lambda^{\alpha_2} - \lambda^{-\frac{\alpha_2}{2}}\right) \quad (7)$$

2.2 Constitutive model verification and simulation analysis

Based on the sample size and load conditions in the experiments, the finite element model of the test sample is shown in Figure 5:

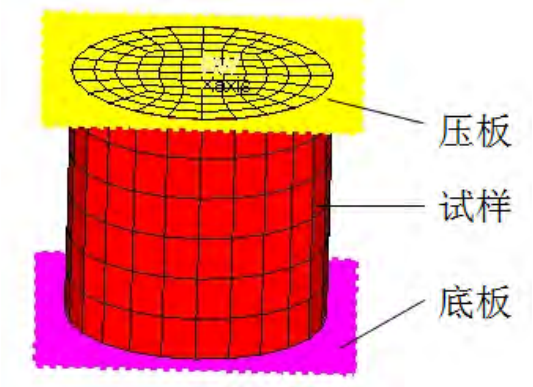

Figure 5 Finite element model of the specimen

Material sample is given 77-O in the finite element model. The force - displacement curves and stress relaxation curves are inputted while strain rate is $20s^{-1}$ according to the test result. Plate is assigned loading time-displacement curve. A set of second-order OGDEN model parameters calculated in LS-DYNA is showed in Table 1. Engineer stress-strain curves of the experiment and simulation while strain rate is $20s^{-1}$ is showed in figure 6.

Material parameter	μ_1	μ_2	α_1	α_2
Value	1.72×10^{-4}	-3.91×10^{-4}	6.63	3.16

Table 1 Simulation model parameter values of second-order OGDEN

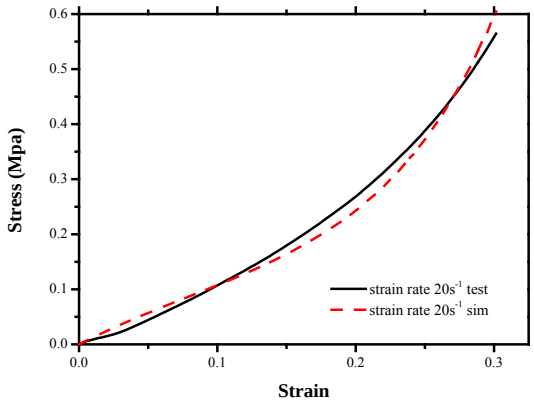

Figure 6 Engineer stress-strain curve while strain rate is $20s^{-1}$

3 Reverse parameter identification procedures

In order to obtain a set of material parameters which lead to better simulation results fitting well with test results, Hybrid genetic algorithm combined with FAE method is used to obtain and refine the μ1，μ2，α1 and α2 in this paper, which are the main parameters of two-order OGDEN rubber model. The minimum difference between engineer stress-strain curve obtained by tests and engineer

stress-strain curve obtained by simulations under $20s^{-1}$ stain rate is taking as the target. LS-OPT software is utilized to find out a group of optimal parameters. Then, these optimal parameters were assigning to FEA model to get engineer stress-strain curves under 0.01 s^{-1},0.1 s^{-1} and 1 s^{-1} strain rate, comparing these curves with testing curves to verify the validity of parameters.

3.1 Feasible Region of Parameters

By running the $20s^{-1}$ strain rate simulation with the LS-DYNA, a set of material parameters are obtained (table 1), which can be regarding as a reference. During the process of optimization, according to the trend of parameters the feasible region needs to be adjusted, the final feasible region of the four parameters is show in table 2.

variable	initial value	Lower limit	Upper limit
μ_1	1.72×10^{-4}	0	4×10^{-4}
μ_2	-3.91×10^{-4}	-5×10^{-4}	0
α_1	6.63	6	9
α_2	3.16	1.5	8

Table 2 Feasible Region of Parameters

3.2 Determination of Object Formulation

The inverse parameter identification procedure is comparing the results obtained by FEA method and the results from tests to acquire the error function. By adjusting the parameters step by step until the error function leads to a minimum, the final optimal parameters can be obtained. According to the algorithms available in LS-OPT, the error function is set like this:

$$\Psi(X) = \frac{1}{m}\sum_{i=1}^{m}\left(\mu_i^{sim}(X) - \mu_i^{exp}\right)^2 \tag{8}$$

where X is the parameter metric unknown, m is the number of testing points, μ_i^{sim} is the FEA simulation response in the ith point testing, $\mu_i^{\exp}$ is the testing response in the ith point testing.

3.3 Hybrid Genetic Algorithm

Hybrid genetic algorithm is a combination of genetic algorithm and frog jumping algorithm [12], which not only has fast calculation speed and excellent global search capability like frog jumping algorithm, but also has the advantages of genetic algorithm. The results are usually better than a separate calculation results using genetic algorithm [13].

1）Put the FEA model under $20s^{-1}$ strain rate into LS-OPT software, allocate the initial values to μ_1，μ_2，α_1，α_2 in two-order OGDEN model and set the variable limits.

2）Use the Sequential with Domain Reduction strategy to conduct 10 iterations, the minimal difference between the responses of the material model and the experimental is set to be the objective; LS-DYNA codes are called an initial solution.

3）Adjust the feasible region of variables and the number of iteration according to the results changing trends caused by different variables, run the codes again and again until the variable converges to a value that is not the border.

4）Decode the optimal individual to obtain the optimal parameters.

The flow chart of this procedure is showed in figure 7. The parameters in table 3 are obtained

by utilizing the above algorithm. The engineer stress-strain curve of strain rate 20 s^{-1}using these optimal parameters is shown in figure 8.

parameter	μ_1	μ_2	α_1	α_2
value	1.82×10^{-4}	-1.16×10^{-4}	8.28	6.28

Table 3 values obtained by inverse identification procedure

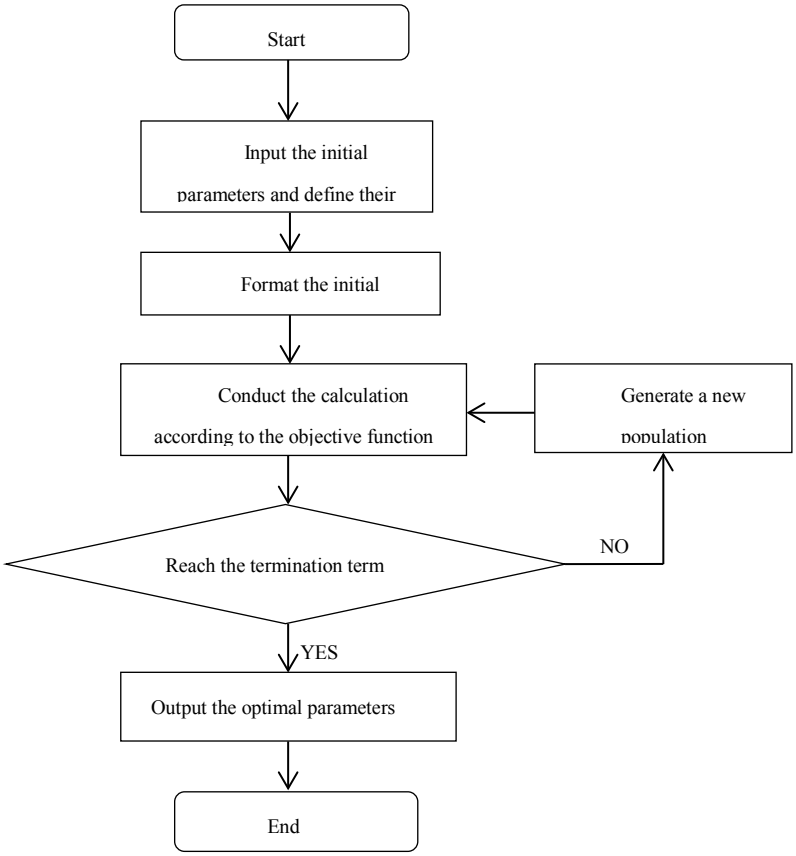

Figure 7 the flow chart of Hybrid Genetic Algorithm optimal procedure

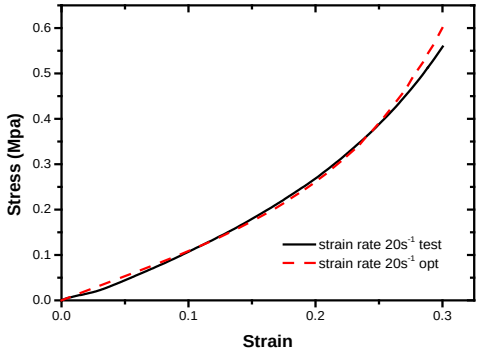

Figure 8 Comparison between optimal and experimental response under $20s^{-1}$ strain rate

Comparing figure 6 with figure 8, it is obvious that there is a big difference between simulation and experimental response under $20s^{-1}$ strain rate in figure 6. Using formulation 8, the number of testing point m=10 was taking uniformly, and the error function value in this case is 2.48×10^{-4}. Figure 8 is the comparison between optimal and experimental response under $20s^{-1}$ strain rate, which shows a better fitting, since the error function value is 1.37×10^{-4}.

3.4 Validation of Optimal Parameter

In order to verify the optimal parameters, the calculations of FAE model under the other three stain rate cases were conduct using the optimal parameters, then comparison between simulation and experimental response was made, if the difference is obvious, rerun the optimization procedure until which leads to a well-fitting result. The engineer strain-stress curves under $0.01s^{-1}$, $0.1s^{-1}$ and $1s^{-1}$ using the optimal parameters above are showed in figure 9 to figure 11.

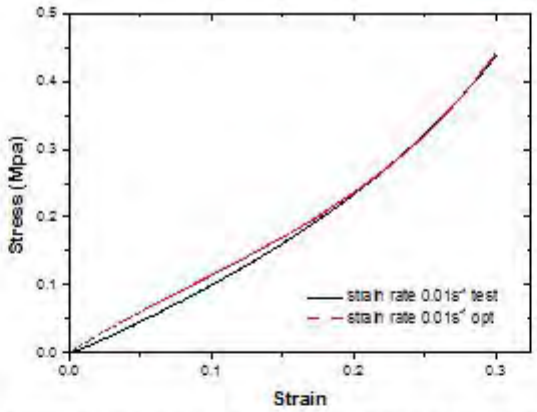

Figure 9 Comparison between optimal and experimental response under $0.01s^{-1}$ strain rate

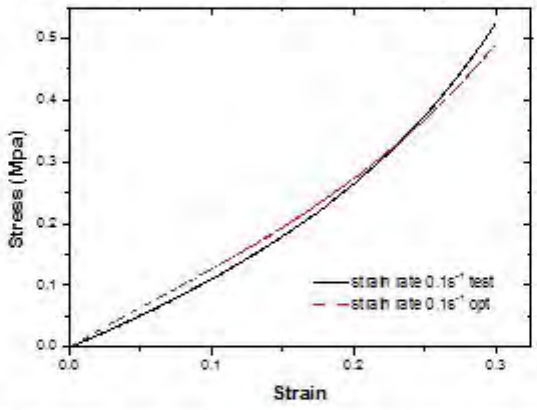

Figure 10 Comparison between optimal and experimental response under $0.1s^{-1}$ strain rate

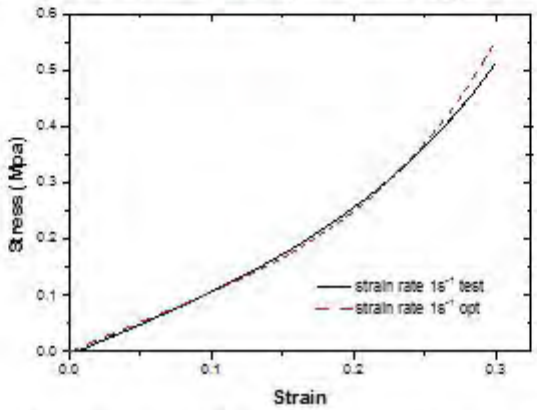

Figure 11 Comparison between optimal and experimental response under $1s^{-1}$ strain rate

Using formulation 8, the number of testing point m=10 was taking uniformly from figure 9 to figure 11, and the error function value is show in table 4. Changing tendencies of parameters (μ_1，μ_2，α_1，α_2) in the optimization process are showed in figure 12.

Strain rate	$0.01s^{-1}$	$0.1s^{-1}$	$1\ s^{-1}$
Value of error function	8.11×10^{-5}	3.41×10^{-4}	1.89×10^{-4}

Table 4 values of error function under different strain rates

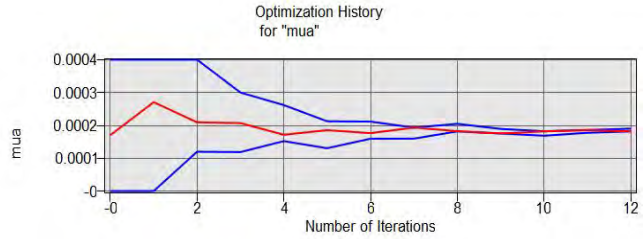

(a) Changing tendencies of parameter μ_1

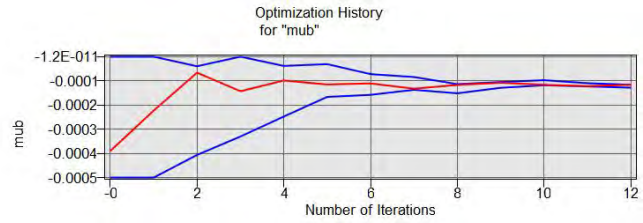

(b) Changing tendencies of parameter μ_2

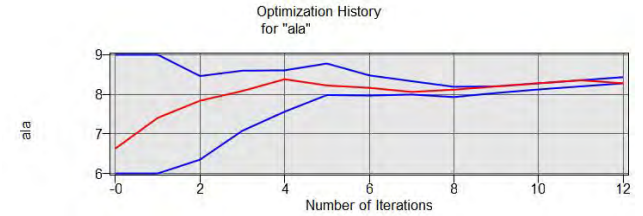

(c) Changing tendencies of parameter α_1

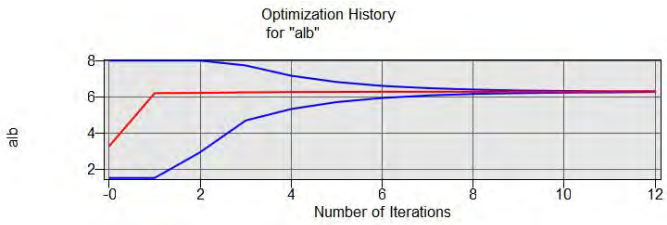

(d) Changing tendencies of parameter α_2

Figure 12 Changing tendencies of the four parameters

Figure 12 and table 4 prove that there is a perfect fit between simulation and experimental response under four different strain rates by using hybrid genetic algorithm. The error function values of ten points are all smaller than 3.5×10^{-4}. The four parameters are stable in non - upper and lower boundaries after 12 iterations, which demonstrate that the parameters using this method are reliable, and it can be used in the dummy skin FAE simulation in the future.

4 Conclusion

This paper focus on material parameters the Hybrid III dummy skin of 40 Shore A solidity, using compressing test under different stains and different strain rates; and combined with FAE simulations, which can be used in dummy simulation with the two-order OGDEN model. Optimal parameters under 20 s^{-1} strain rate based on inverse parameter identification procedures have a

well-fitting with experimental response. The parameters of different solidity used in the dummy under different strain rates will be done utilizing the same method in the future.

Reference

[1] Yu Xiang, Yuan Zhongfan, Guo Zuoda,et al. Research on the Technics Experiment Dummy for Obverse Impact on Automobile[J]. Journal of SiChuan University (Engineer Science Edition) 2002,34(3):119-123

[2] Zhang Chunhong, Lin Daquan. Analysis of bionic technologies of anthropomorphic phantom in China[J]. Machinery, 2009,1(36):1-4

[3] Xie Chi, Cai Peng, Lin Daquan, et al. Impact Performance Analysis of Car Crash Test for Dummy Bionic Skin Material [J]. Chinese Journal of Automotive Engineer, 2011,01(z1):126-129.

[4] Sai S. Sarva, Stephanie Deschanel, Mary C. Boyce, et al. Stress-strain behavior of a polyurea and a polyurethane from low to high strain rates [J]. Polymer, 2007 (48) :2208-2213

[5] Garrett W. Wood, Matthew B. Panzer, Cameron R. Bass, et al. Viscoelastic Properties of Hybrid III Head Skin [J]. SAE International,2010, 01(0383):186-193

[6] John Z. Wu, Ren G. Dong, W. Paul Smutz, et al. Nonlinear and viscoelastic characteristics of skin under compression: experiment and analysis[J]. Bio-Medical Materials and Engineer, 2003 (13): 373–385

[7] C.M. Roland, J.N. Twigg, Y. Vu, et al. High strain rate mechanical behavior of polyuria [J], Polymer, 2007 (48) 574-578

[8] V. Delhaye, A.H. Clausen, F. Moussy, et al. Influence of stress state and strain rate on the behaviour of a rubber-particle reinforced polypropylene [J]. International Journal of Impact Engineer, 2011(38):208-218

[9] Rubber, vulcanized-Determination of creep in compression or shear[J]. BRITISH STANDARD.BS ISO 8013:2006

[10] Lu Chunhong, Bai Hongbai. Study on Constitutive Model of Viscoelastic Material[J]. Polymer Materials Science and Eengineer,2007,23(6):28-32

[11] S. Reese, P. Wriggers. A material model for rubber-like polymers exhibiting plastic deformation: computational aspects and a comparison with experimenral results[J]. Computer methods in applied mechanics and engineer,1997(148):279-298

[12] Gareth P. Harrison, Antonio Piccolo, Pierluigi Siano, et al. Hybrid GA and OPF evaluation of network capacity for distributed generation connections [J]. Electric Power Systems Research , 2008 (78) :392–398

[13] Nielen Stander, Willem Roux, Tushar Goel, Trent Eggleston, et al. LS-OPT User's Manual-A Design Optimization and Probabilistic Analysis Tool for the Engineer Analyst[R]. Livermore Software Technology Corporation,2012:408-413

Development of a Database of Advanced Material Properties for LS-DYNA

Prof. Dr. Viktor Pocajt, Jason Zhai

(Key to Metals AG, Switzerland)

Abstract This paper describes a development of a large database of advanced material properties for metallic materials, and more recently polymers, ceramics and composites. This new database, which relies on a proprietary methodology that combines property acquisition and assessment, has a specific aim of serving the global engineering community with mechanical and physical properties needed for advanced CAE (Computer Aided Engineering) and FEA (Finite Element Analysis) calculations and simulations.

In the database, advanced material properties have been divided to (1) stress-strain curves, (2) formability curves, (3) cyclic properties, (4) fracture mechanics, and (5) creep properties. The biggest challenge in providing these properties for a large number of engineering materials and service conditions is a general scarceness of experimental data. Besides collecting and consolidating information for more than 100.000 datasets from more than 1.200 references, a specific set of algorithms has also been developed for streamlining and assessing/interpolating properties under various conditions (service temperature, heat treatment etc.).

Keywords: material properties, metals, polymers, composites, stress-strain curves, cyclic properties

1. Introduction

The importance of accurate material properties information for engineering calculations and simulations can never be overstated. Even conventional mechanical properties such as yield strength, tensile strength, hardness, and ductility may vary more than tenfold for structural steels at room temperature, depending on the variations of alloying elements, heat treatment and fabrication. With a moderate change in working temperature, the subsequent property variation and associated changes can become even more profound and their approximations may lead to very serious errors. In fact, this lack of accurate information concerning material properties poses one of the highest risks in structural design, accounting for over 29% of structural failures [1].

The main mechanical properties such as yield and strength, hardness, ductility, and Young modulus are included within the standard dataset of Key to Metals database, together with international cross-reference tables, composition, physical properties, and more. However, while these properties generally suffice for conventional calculations within the elastic range, they cannot fulfill the needs of advanced calculations that include plasticity, fatigue and fracture mechanics, needed for the most demanding CAE simulations [2].

Extended Range is a new part of the Key to Metals database, specifically designed to compile

advanced mechanical properties information, which is typically very hard to find. Advanced mechanical properties have been divided into (a) stress-strain curves, (b) formability curves, (c) cyclic properties, (d) fracture mechanics, and (e) creep properties. The biggest challenge in providing these properties for a large number of materials and service conditions is a general scarceness of published experimental data. To overcome this problem, in the process of database development over 1,200 data resources have been acquired, ranging from relatively large data collections [3] to individual papers dating back from over 50 years ago [4] to more recent documents [5]. In addition, an innovative methodology has been developed for integrating raw data obtained from diversified experiments from all over the world, consisting of a specific set of algorithms for data selection, processing and assessment for each of the five advanced properties modules, Figure 1.

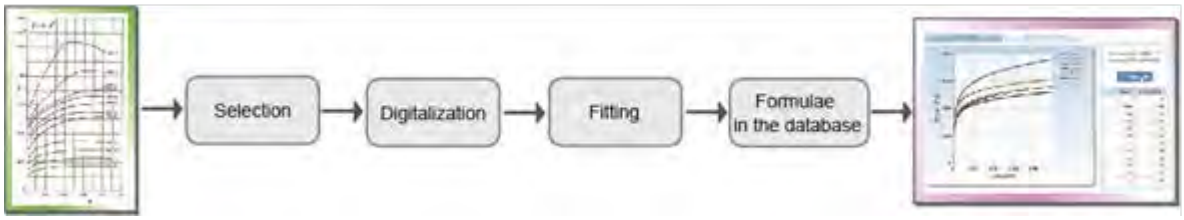

Fig. 1. The workflow for processing experimental results.

Since its introduction in 2011, the Extended Range database has gained significant popularity in the CAE community and in turn its application in various fields of CAE simulation has enabled dynamic further development. Besides an increase in the number of records and materials covered, a number of new features have been added, such as formability stress-strain curves, estimation of Wohler curves, statistical fatigue parameters and more [2]. Significant recent developments also include new methods for assessing advanced material properties, which will be briefly described in this paper.

2. Stress-Strain Curves

Stress-strain curves are of particular importance for calculations that include plasticity either in static or in dynamic loading, e.g. for controlled plastic deformation, autofretage, forging, crash behavior and other areas of simulation. There are a relatively low number of materials for which experimental curves have been made, and even this information is hard to find. When found, the information is often in a form inconvenient for use, e.g. graphs on the paper. In addition to this, it is delicate to find and error-prone to assess properties under various conditions, such as working temperature, strain rate, and heat treatment.

Applying the methodology outlined in Figure 1, after digitizing using a strictly controlled process, a combination of Ramberg-Osgood and Ludwik equations is applied on the set of obtained data points [6], together with a range of temperature-dependent physical properties like Young modulus. Using this methodology, equations that represent the best fit are obtained for various temperatures, strain rates and delivery conditions, depending on the available experimental data. The coefficients of the equations are embedded in the database, so the stress-strain curve can be created and displayed in real-time, or can be automatically recalculated for user defined working temperatures, Figure 2. As a result of this process, more than 40,000 stress-strain curves have been

defined for about 3,600 materials; for many of them there is also a range of working temperatures and conditions available, which can account for over 100 curves for a single material.

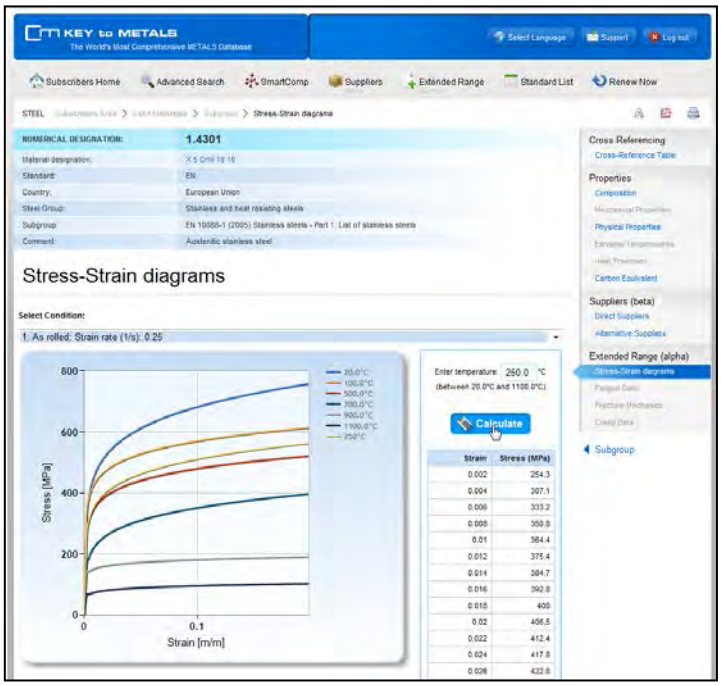

Fig. 2. An example of stress-strain curves, with a calculation of a curve for user-defined working temperature.

3. Fatigue Data

Cyclic properties have also been processed using proprietary methodology, both for strain and stress life. In order to compile cyclic properties for a substantial number of materials, an extensive literature review project has been completed as an initial step. Although the scope of the project was large, available experimental data on cyclic properties is sparse. As with stress-strain data, the information is often presented in a format inconvenient for use and often created from a material that has been subjected to specific experimental conditions such as working temperature, strain rate or heat treatment leading to the potential for error in applying them for the concrete engineering structure or simulation.

Therefore, a workflow similar to that in Figure 1 was created which has resulted in fatigue data for more than 4.500 metallic alloys, again with multiple datasets where available, for different heat treatments and loading conditions. Statistical parameters have been provided where applicable, as well as graphical presentation of the data, Figure 3. The implemented graphs have been made interactive and the values of strain or stress amplitude versus number of cycles are displayed as the user moves the mouse cursor over the graph.

Fig. 3. An example of strain-life fatigue data.
Monotonic properties are provided for reference.

4. Advanced Material Properties Assessment

Due to a general scarcity of experimental data, even a database as large as Key to Metals Extended Range containing several thousand materials covers advanced properties information for only a relatively small part of all standardized and proprietary structural materials that are being used worldwide, the total number of which can be roughly estimated at more than 300.000.

As a new alternative method for properties assessment, the Key to Metals database provides a possibility to quickly and easily estimate unknown advanced properties of a material alloy using advanced properties of similar materials that are derived from the Key to Metals cross-reference tables. These tables of equivalent materials come from the recommendations of Standards Development Organizations (SDOs), literature and other sources. Since over 10 million cross-reference records are readily available within the Key to Metals database, the implementation of this approach is relatively straightforward and provides users with estimates of advanced properties for an additional 30.000 materials.

An example of such an estimate is given in Figure 4. The original material, in this case Chinese steel Q235, does not have stress-strain curves available, but its European equivalent S235JRG2 does, so the stress-strain data of S235JRG2 can be used as an estimate for Q235. It should be noted that, regardless of the fact that the materials are declared equivalent, the user can check the similarity of the properties for the two materials by using a side-by-side comparison view and eventually decide whether the similarity between materials is sufficient for the particular application in mind.

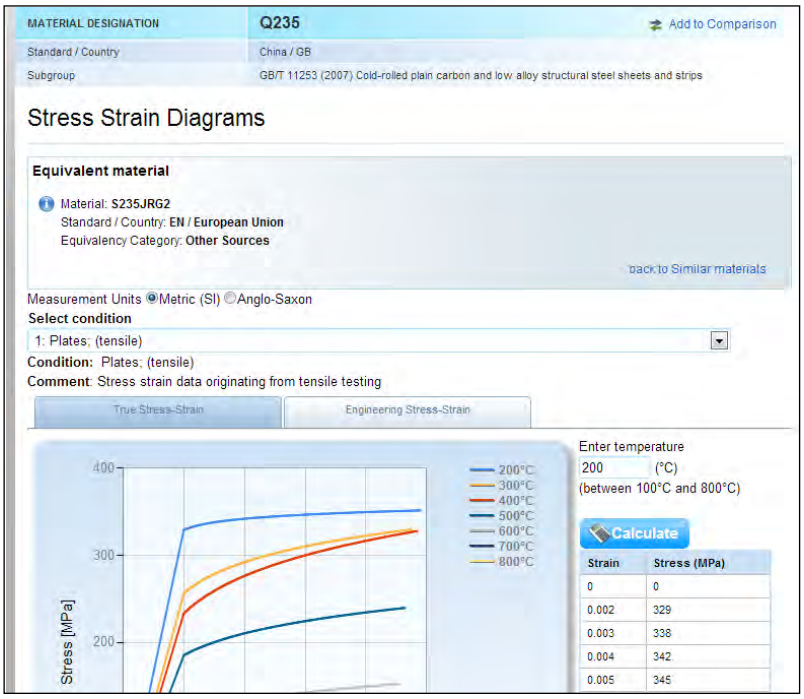

Fig. 4. An example of stress-strain curves of an equivalent material to Chinese Q235.

Of course, properties derived using similar materials cannot represent an ultimate solution or a replacement for experiments, but they can provide a useful starting point for further research and simulations. Initial benchmarking for delicate cyclic properties showed that using cross-reference tables to assess properties provides estimates that are at least comparable to those of other methods [8].

In addition, a new fuzzy-logic based module SmartCross^2 has been developed. Using a proven, patented algorithm for the identification and comparison of metals [9], SmartCross^2 is designed to find unknown equivalents by composition, mechanical properties, or any combination thereof autonomously, that is without user intervention. Once the list of “candidates” for similar materials is obtained, they can again be used to estimate advanced properties.

5. Integration possibilities with CAE software

An increased usage of Key to Metals and especially Extended Range module in CAE analysis has recently led to an increased number of requirements for some form of integration with CAE software. While implementation of such integration and its complexity level can depend on a number of technical and contractual questions, in recent months a few relatively simpler solutions have been developed in order to provide a higher level of accuracy and time savings to CAE engineers.

An example of loose integration is a customized solution developed for a CAE software vendor, where the CAE user has a possibility to select certain properties, manipulate them and export in an ANSYS-compatible MatXML file format, and the obtained file can then be used for populating an internal ANSYS material database. The functionality has been implemented as a desktop application, an add-on to the Key to Metals Desktop Edition, Figure 5 [9]. A similar set-up has been developed for Altair Hyperworks users on the Web platform, with a possibility to export data either in XML

format or directly in a solver format. The LS-DYNA material export format is under development with Shanghai Hengstar for Chinese users.

Fig. 5. An example of desktop interface for data export.

Since they substantially reduce time and effort in finding material properties and inputting them to the solvers, and in the same time increase accuracy and reduce possibilities for input errors, these exporting functionalities got very positive feedback from CAE users. Therefore, a development of new module eXporter is started, that will, instead of se custom-developed export for a single solver, provide material property data export possibility to a majority of most popular CAE solvers, enabling the user to select data online and export it to the solver of multiple solvers of his current interest.

5. Conclusions

As a consequence of a permanently increasing demand for accurate and reliable material properties data that can be used for sophisticated CAE analysis and simulations, the database of advanced material properties Extended Range has undergone very dynamic development that included an increased number of records and materials covered, and a number of new features added, such as formability stress-strain curves, estimation of Wohler curves, statistical fatigue parameters, new families of stress-strain curves, new methods for assessing advanced material properties, and integration possibilities with CAE software such as LS-DYNA.

Besides further increase of data in the existing modules, on-going and future developments are focused to extending the data coverage for polymer, ceramic, composite and nano materials, including data needed for diversified material models such as orthotropic materials. Also, a completely new module for joints is being developed that can help CAE engineers to get a quick insight into properties of welded, soldered, glued and mechanical joints of metals and non-metals.

Future developments planned also include tighter integration with most popular CAE software packages, with an idea to use the complete data scope of the Key to Metals database from within the

CAE tool, by the means of Web services that will be called by the CAE tool on an as-needed base.

References

[1] Radovic, A., Radovic, N., 2004. In: From Fracture Mechanics to Structural Integrity Assessment, Society for Structural Integrity and Life, Belgrade, pp. 83-90.

[2] Pocajt, V., Baumann, N., 2012. Development of a Database of Material Properties for CAE. NAFEMS 2012 UK Conference, Lincolnshire, May 2012.

[3] Doege, E., Meyer-Nolkemper, H., Saeed. I., 1986. Fliesskurvenatlas metallischer Werkstoffe: mit Fliesskurven für 73 Werkstoffe und einer grundlegenden Einführung. ISBN: 3-446-14427-7. München: Hanser.

[4] Hughes, P.J., Inge, J.E., Prosser S.B., 1955. Tensile and compressive stress-strain properties of some high-strength sheet alloys at elevated temperatures. NACA Technical Notes, No 3315.

[5] Pla-Ferrando R., Sánchez-Caballero S., Selles, M.A., Martínez-Sanz A.V., 2011. TWIP/TRIP Steels. Future Trends in Automotive Industries. Annals of the Oradea University, Fascicle of Management and Technological Engineering, Volume X (XX), pp. 1.23-1.26.

[6] Skrzypek, J. J., 1993. Plasticity and Creep. Theory, Examples, and Problems. ISBN 0-8493-9936-X. Boca Raton, FL: CRC Press.

[7] Pocajt, V., Ogarevic, V., 2010. Estimation of mechanical properties of metals on the example of fatigue characteristics. 33 Convegno Nazionale AIM (in Italian), Brescia, November 2010.

[8] Pocajt, V., Sevarac, Z., Kovacevic, A., 2009. SmartMetals: A New Method for Metal Identification Based on Fuzzy Logic. Journal of Chemometrics, Volume 23 (11), pp. 555-561.

[9] Sasaki, T., 2012. A New Software for Exporting Material Properties to ANSYS Workbench. Cybernet Users Meeting, September 2012, Tokyo, Japan.

Nonlinear Crashworthiness Optimization integrated with LS-DYNA and Equivalent Static Load method

Feng Pan[1]，Renwei Hu[1]，Phani Adduri[2]，Gary Quinn[2]

（1 Shanghai Hengstar Technology Co., Ltd., Shanghai, 201203, panfeng@hengstar.com）

（2 Vanderplaats Research & Development, USA）

Abstract： This paper illustrates the use of ESLDYNA to couple with LS-DYNA and GENESIS for performing a vehicle frontal crashworthiness optimization to minimize the intrusion of the firewall into the passenger compartment. Topometry optimization is used to modify individual shell element thicknesses in the designable region of the auto body structure with 5,200 design variables. The whole optimization process takes only five LS-DYNA simulations and twenty-five GENESIS design iterations to reach good optimization results. This integrated method makes it possible for engineers to increase the safety of their vehicle designs with a minimum computation effort. ESL-based optimization is an ideal way to solve large-scale optimization problems in practice.

Keywords: Crash optimization; LS-DYNA; GENSIS; Equivalent Static Load

Continuous strict standards for safety and fuel efficiency have been a great boot to vehicle crashworthiness and lightweight design, becasue there is a contradiction between these requirements. Development of the computational power and advancements of numerical algorithm make it possible to simulate a large-scale automobile model. In this way, it helps augment the crash test and also gives engineers insight into crash events. These nonlinear simulations have become commonplace during the design phase to save time and cost. However, automobile crash optimization still has difficulties due to the high cost of calculating sensitivity of design variables. Also, impact simulation and analysis require extensive computational resources. As a result, there is a growing interest in using metamodel (also called surrogate model), by constructing an approximation model of the complicated highly non-linear problems based on a limited selection of results from a computationally high-fidelity crash simulation to deal with the analysis and optimization process[1]. Metamodels such as polynomial response surface, kriging, radial basis function, support vector regression has been widely used in engineering application to alleviate the computational burden and conduct design space exploration and optimization with the help of several commercial toolkits like LS-OPT, VisualDOC etc. Although it is possible to coupling crash simulation with a standalone optimization program (using design of experiments and metamodels) to improve crash performance in practical applications, it seems that they may be successful in problems with a small number of designable parameters, usually less than 10 variables[2], because of the accuracy of the metamodels constructed.

Most publications on vehicle crash optimization used efficient design techniques and sampling strategies. But it has two major limitations[3]. First, it is difficult to match the exact performance of the full-scale original model accurately to the metamodel. The precision varies according to the selection of the approximation method and the model. Yang et al.[4] compared the performance of stepwise regression, moving least squares, kriging, multi-quadratic adaptive and interactive modeling systems. They concluded that there is no single metamodel that can fit all the impact functions and that further development of a hybrid modeling strategy is needed. Second, there is a limitation on the number of design variables. The increment in the design variables reduces the precision of the metamodel and requires many non-linear crash simulations. Besides, general-purse optimization toolkits for practical reasons may support size and shape optimization. Some powerful techniques such as topology, topography, and topometry type optimizations, which require a large of design variables, are not feasible in the general-purpose optimization for nonlinear problems. Thus, a large-scale crash optimization which has many designable parameters is rarely solved.

In order to overcome these difficulties and limitations, the equivalent static load (ESL) method has been proposed by Park[5]. ESL method can considerably improve the accuracy of optimum solution because a gradient-based optimization method is utilized in the design optimization process. This method is not sensitive to the number of design variables because it uses the linear static response optimization method. ESL is defined as the load sets which generate the same response field in linear static analysis as that from each time step in nonlinear dynamic analysis. Nonlinear dynamic response optimization is conducted by repeated use of linear static response optimization. ESLDYNA is an implementation of the ESL method to seamlessly perform optimization based on an LS-DYNA nonlinear analysis with GENESIS as the structural optimization program.

In this paper, a brief introduction of ESL method is reviewed, followed by the ESLDYNA plug-in toolkit for combining GENESIS and LS-DYNA. One demonstrative case for frontal crash optimization is used to show the applicability of ESLDYNA.

1 Review of Equivalent Static Load Method[5]

The conventional formulation of nonlinear dynamic response structural optimization can be expressed as follows:

$$\begin{aligned} &\textit{Minimize}: \ F_{obj}(\mathbf{b},\mathbf{z}) \\ &\quad S.t.: \ \mathbf{M}(\mathbf{b})\ddot{\mathbf{z}}_N(t)+\mathbf{K}_N(\mathbf{b},\mathbf{z}_N(t))\mathbf{z}_N(t)-\mathbf{f}(t)=0 \\ &\qquad t=t_0,t_1,t_2,...,t_n \\ &\qquad g_j(\mathbf{b},\mathbf{z}_N(t))\le 0, \ \ j=1,...,l \\ &\qquad b_{iL}\le b_i\le b_{iU}, \ \ i=1,...,m \end{aligned} \tag{1}$$

where **M** is the mass matrix which is the function of the design variable vector **b**. **K** is the stiffness matrix which is the function of the design variable vector **b** and the nodal displacement vector **z**, and $\ddot{\mathbf{z}}$ is the acceleration vector. N means that the response is obtained from nonlinear analysis. Since it is nonlinear optimization, governing equation of nonlinear dynamic analysis using finite element method should be satisfied as shown in above formulation. *n* is the total number of time step. *l* and *m* are the numbers of the constraints and design variables, respectively. **f**(*t*) is the external load vector at the t^{th} time step.

From the formulation, dynamic response optimization can have many time dependent constraints with total number of constraints of $n \times l$. Since the calculation of the sensitivity considering the incremental step is extremely difficult, it is rare to perform nonlinear dynamic response structural optimization for large scale problems.

The equivalent static load (ESL) is defined as the static loads which generate the same response fields in linear static analysis as those of nonlinear dynamic analysis at an arbitrary time. Figure 1 illustrates the concept of ESL. An equivalent load set is made for each time step of nonlinear dynamic analysis. The linear static response from the i^{th} equivalent static load is the same as the nonlinear dynamic response at the i^{th} time step. Thus the total number of time steps is equal to the total number of equivalent static load sets, and the profile of the static response which is generated from linear static analysis using equivalent static loads is exactly the same as the dynamic response profile from nonlinear dynamic analysis. In other words, if s_i equivalent static loads are used as external forces in linear response analysis, the response is the same as the response of the t_i^{th} time step of nonlinear dynamic analysis.

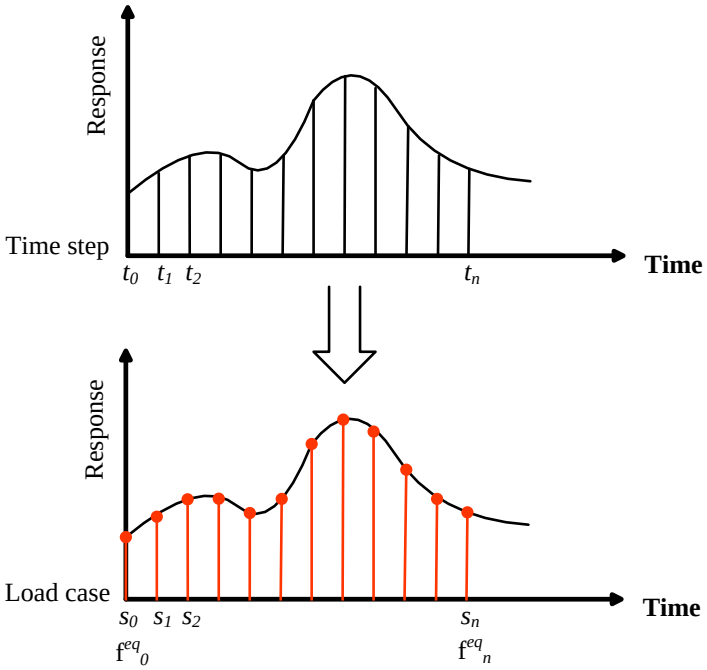

Figure 1: Concept of ESL at every time step

In the finite element method, the equilibrium equation of a structure in the time domain with nonlinearity is

$$\mathbf{M}(\mathbf{b})\ddot{\mathbf{z}}_N(t) + \mathbf{K}(\mathbf{b}, \mathbf{z}_N(t))\mathbf{z}_N(t) = \mathbf{f}(t) \quad where\ t = t_0, t_1, t_2, ..., t_n \tag{2}$$

we do not consider damping effect in the method introduction. The equivalent static load for displacements in defined as

$$\mathbf{f}^{\mathbf{z}}_{eq}(s) = \mathbf{K}_L(\mathbf{b})\mathbf{z}_N(t) \quad where\ s = s_0, s_1, s_2, ..., s_n \tag{3}$$

where s is exactly matched with t. n equivalent static loads are obtained from Eq.(3). $\mathbf{f}^{\mathbf{z}}_{eq}(s)$ is

computed by multiplying the linear stiffness matrix $\mathbf{K}_L$ and the nodal displacement vector $\mathbf{z}_N(t)$.

If $\mathbf{f}_{eq}^{\mathbf{z}}(s)$ is used as an external force which is the equation of linear static analysis

$$\mathbf{K}_L(\mathbf{b})\mathbf{z}_L(s) = \mathbf{f}_{eq}^{\mathbf{z}}(s) \tag{4}$$

the nodal displacement vector $\mathbf{z}_L(s)$ has the same values as the nonlinear nodal displacement vector $\mathbf{z}_N(t)$ at an arbitrary time. The equivalent load sets are used as multiple loading conditions in the linear static response optimization. Therefore, the flowchart of ESL-based optimization can be illustrated as follows:

a) Nonlinear analysis to solve the response;
b) Obtain the equivalent static loads which reproduced the equivalent responses;
c) Solve a linear structural optimization using ESL;
d) Judge convergence condition. If not, update the FE model for nonlinear analysis.

2 ESLDYNA

As reviewed in above section, it is obvious that vehicle crashworthiness optimization is typical nonlinear analysis and ESL method can be used to perform different kinds of optimization. For example, nonlinear responses such as nodal displacements, accelerations, and energies are calculated from LS-DYNA. GENESIS, a linear structural optimization code from Vanderplaats Research & Development (VR&D), is used to optimize these responses. Therefore, the FE meshes in each data format (both in LS-DYNA and GENESIS) need to be prepared to run both codes. The general flowchart is as follow, and also shown in Figure 2[6].

a) LS-DYNA must be run to obtain responses (e.g., displacement fields) and they must be output in a result file (e.g., nodout or binout);
b) ESL must be calculated using the obtained responses, which can reproduce the exact same responses in the GENESIS analysis;
c) Structural optimization will be performed using GENESIS using ESL. During optimization, if the model (e.g., size, shape, topology) is changed, ESL is no longer equivalent since LS-DYNA does not produce the same responses with an updated model obtained by the GENESIS optimization.
d) Then it is required to re-calculate the nonlinear responses using the updated FE model and repeat the process of optimization until a convergence condition is met.

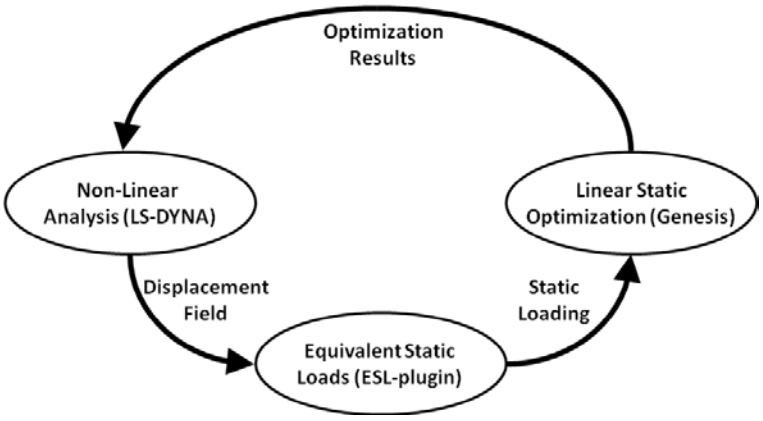

Figure 2: Flowchart of ESL based optimization using LS-DYNA and GENESIS

GENESIS is a fully integrated finite element analysis and optimization software. Analyses include static, normal modes, direct and modal frequency analysis, heat transfer, system buckling, and random response. Shape, sizing, topography, topometry, topology, and freeform optimization are the design options available to the user. Typically the optimization requires less than ten finite element analyses to converge even for large problems with the help of GENESIS.

ESLDYNA is also available as a plug-in in Design Studio for GENESIS (DSG) to combine LS-DYNA analysis and GENESIS optimization, as shown in Figure 3. Most of the different types of design optimization techniques in GENESIS are available for designing the nonlinear model. Multiple loading conditions in the nonlinear analysis, using several LS-DYNA input files, can be analyzed simultaneously to achieve optimal solutions. This plug-in provides an easy to use interface with seamless integration between GENESIS and LS-DYNA, thus the user does not need to use the *PARAMETER cards etc. to modify the input deck. The plug-in can prepare the updated LS-DYNA file for every iteration.

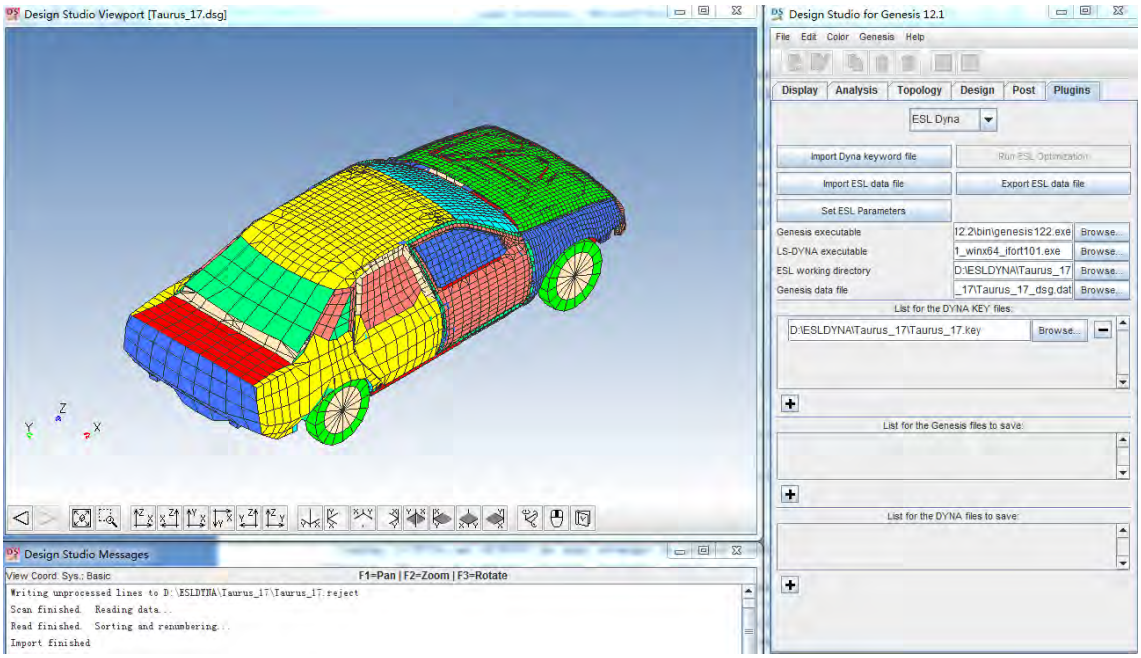

Figure 3: ESLDYNA plug-in Interface

Coupling LS-DYNA and GENESIS has many advantages for nonlinear crashworthiness

optimization. The use of traditional non-linear optimization method (usually called as Metamodel-Based Design Optimization, MBDO) relies on exploration of the design space, which inherently requires LS-DYNA to be called by the optimizer for acquire sensitivity data. In ESLDYNA, the sensitivity of design variables can be calculated internally within GENESIS, so the number of LS-DYNA function calls can be reduced largely. This in turn removes the link between design variables and functions calls, and dramatically increases the number of design variables that can be considered. Figure 4 shows a comparison study between MBDO method and the ESLDYNA plug-in method to solve the same problem. It indicates that the relationship between the number of design variables and the number of LS-DYNA runs. The figure shows positive correlation for MBDO method, whilst there is no obvious correlation for ESLDYNA plug-in.

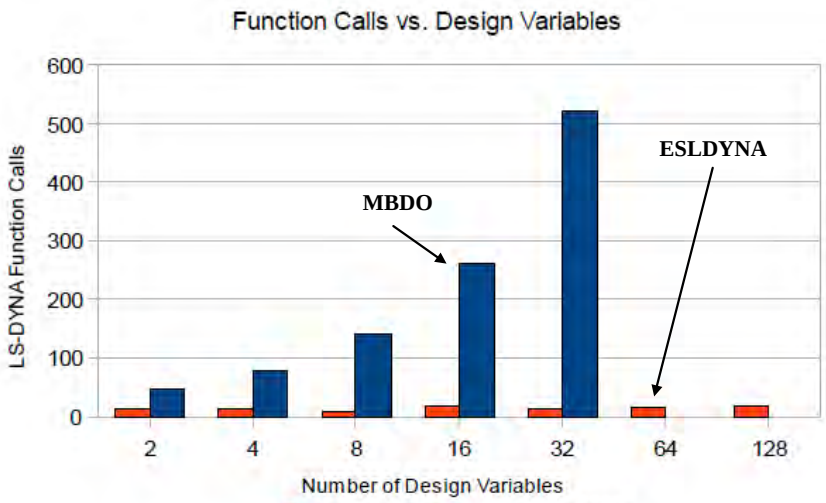

Figure 4: Comparison of function calls for MBDO and ESLDYNA[7]

3 Vehicle Crashworthiness Optimization

Crashworthiness design is the most difficult task for vehicle development. LS-DYNA is widely used in crash simulation around the world. The demo case intends to apply ESLDYNA to perform the nonlinear crashworthiness optimization. A full-overlap frontal crash of Taurus is used with total calculation time of 150ms, as shown in Figure 5. The whole FE model is used as GENESIS input file. We fixed the degrees-of-freedoms for the wheels and bumper locations, as shown in Figure 6.

In this case, the objective is to minimize the firewall intrusion into the passenger compartment. Eight points on the firewall were selected to measure the intrusion, as illustrated in Figure 7. Equivalent static loads can be defined for any number of LS-DYNA time points (e.g., t=75ms in this case). In this case, topometry optimization is used to modify individual shell element thicknesses in the designable region as shown in Figure 8. The thickness of each element is set up to vary from one half to two times their initial thickness. The total number of design variables is 5,200. For constraints, the total mass is only allowed to change by plus or minus 10kg.

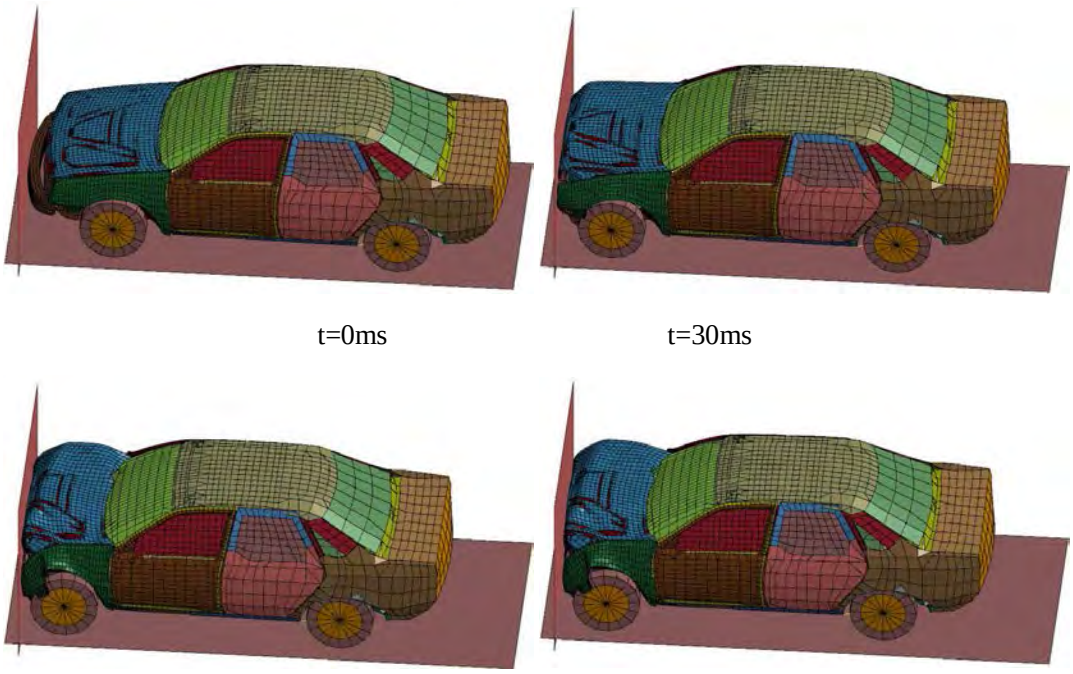

t=0ms t=30ms

t=60ms t=120ms

Figure 5: Taurus model for frontal crash

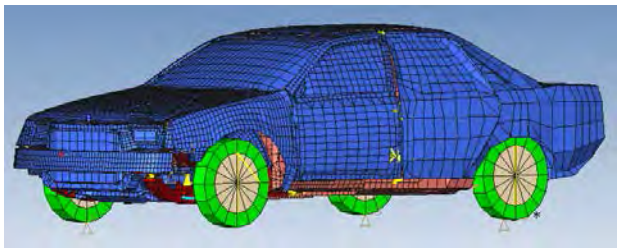

Figure 6: Genesis input file

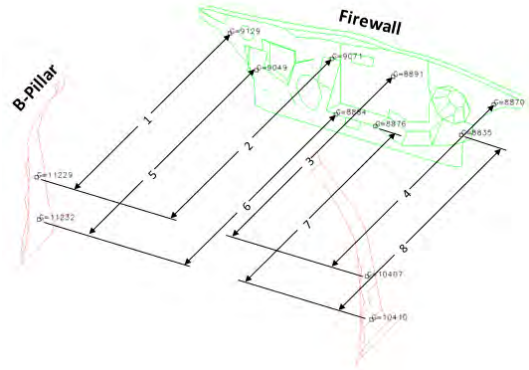

Figure 7: Firewall intrusion measure

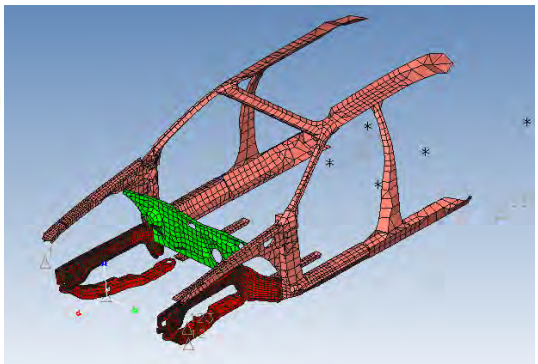

Figure 8: Designable variables

Figure 9 shows the convergence history of objective and constraint functions, in which the objective function is synthetic response based on the intrusions of eight points on firewall. The optimization process took 10 LS-DYNA simulations and 50 GENESIS design cycles to complete. LS-DYNA simulates averaged 40mins each while GENESIS design iterations averaged 20mins each. This shows the benefits of using ESL method for nonlinear crashworthiness optimization obviously. Most ESLDYNA problems, including this case, give good optimization results after only five LS-DYNA simulations and 25 GENESIS design iterations.

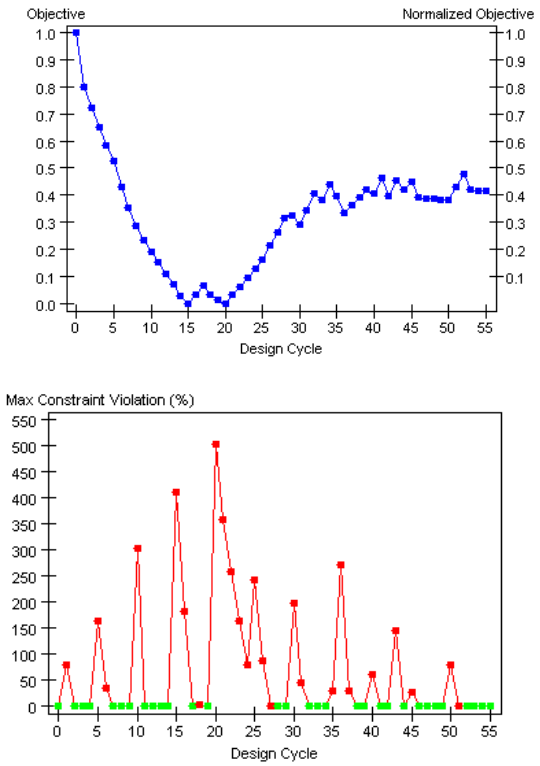

Figure 9: Convergence history of objective and constraint functions

The initial and optimized shell thicknesses are shown in Figure 10. The results indicate the parts of A-pillar have the thickest shell elements at around 3.5mm. Connecting parts between A-pillar and roof rail are also have large thickness around 5mm. The final design cycle shows that optimized element-by-element thickness distribution that limits firewall intrusion into passenger compartment during a frontal crash simulation. From the topometry optimization results, it can give guideline and suggestions for engineers to re-design the structures to improve the crashworthiness.

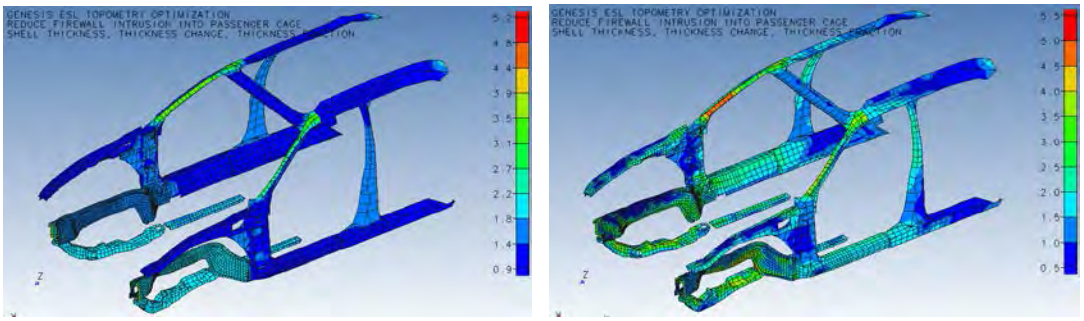

Figure 10 Shell thickness distributions for initial thickness (left) and optimized thickness (right)

Figure 11 compares the LS-DYNA final deformation at 150ms for the initial design versus the optimized design. The structural deformation mode is similar for initial design and optimized design. However, the max point intrusion among 8 measured points is largely reduced after topometry optimization. Relative displacement results of 8 intrusion points are taken from LS-DYNA crash analysis, which is shown in Figure 12. It illustrates that intrusion of the firewall into the passenger compartment has been reduced at all eight measured points. For example, the intrusion of point 5 is reduced by about 80%, from 64.6mm to 13mm, which indeed will help to improve the occupant safety. For optimized design, the total mass of whole vehicle is increased by 9.7kg.

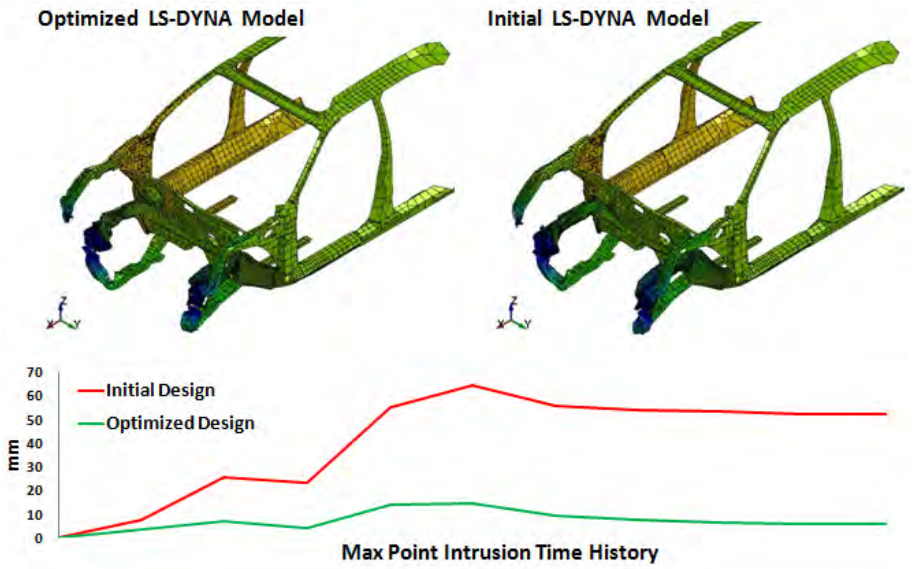

Figure 11: Comparison of max point intrusion of firewall

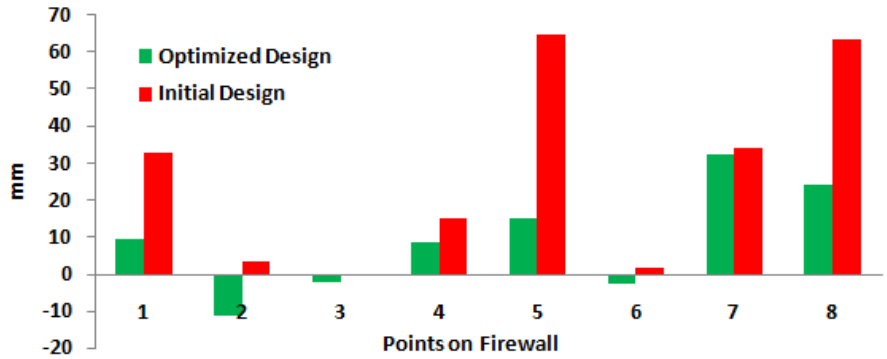

Figure 12: Max Firewall Intrusion into Passenger Compartment

4 Conclusions

By coupling LS-DYNA and GENESIS, it is possible to perform nonlinear crash optimization directly. This method can achieve an optimum design quickly with less number of LS-DYNA simulations and GENESIS design iterations, while total computational cost is almost the same even for a great number of design variables. With the help of ESLDYNA, it is very convenient to set up nonlinear structural optimization case as the demo case of frontal crash optimization was illustrated. Due to powerful optimization techniques of GENESIS, ESLDYNA can also support sizing, shape, topology and freeform optimization besides topometry. Note that topology can't be worked with other type of optimization techniques simultaneously. Therefore, ESL based optimization is an ideal way to solve large-scale optimization problems in practice.

Reference

[1] Pan F, Zhu P. Design optimisation of vehicle rood structures: benefits of using multiple surrogates. International Journal of Crashworthiness 2011:16(1):85-95.

[2] Zhu P, Pan F, Chen W, Viana FAC. Lightweight design of vehicle parameters under crashworthiness using conservative surrogates. Computers in Industry 2013:64(3):280-289.

[3] Jeong S, Yoon S, Xu S, Park G. Non-linear dynamic response structural optimization of an automobile frontal structure using equivalent static loads. Proceedings of the Institution of Mechanical Engineers, Part D: Journal of Automobile Engineering 2010:224(4):489-501.

[4] Yang R, Wang B, Wang N, Tho C, Bobineau J. Metamodeling development for vehicle frontal impact simulation. Journal of Mechanical Design 2005:127(5):1014-1020.

[5] Park G. Technical overview of the equivalent static loads method for non-linear static response structural optimization. Structural and Multidisciplinary Optimization 2011:43:319-337.

[6] Kosaka I. Improvement of energy absorption for the side member using topography optimization. 11th International LS-DYNA Users Conference, 2010.

[7] Salway D, Pierre P, Liebscher M. Practical examples of efficient design optimization by coupling VR&D GENESIS and LS-DYNA. 7th European LS-DYNA Conference, 2009.

Isolation scheme assessment on the Raffles City Chongqing using LS-DYNA

Francois Lancelot, Robin Ching, John Hand

（Arup）

Abstract：The super-scale development of Raffles City Chongqing embodies the rise of Western China. This mega-complex, comprising a shopping mall and 8 mixed-use towers has been designed by the internationally acclaimed architect Moshe Safdie for the developers CapitalLand and Singbridge Holdings. Arup has been appointed to provide structural engineering services for all design stages.

The 400m long conservatory that bridges the four interior towers at the 60-storey level presents particular engineering challenges.

At the concept stage, nonlinear time-history seismic analyses of the towers and conservatory have been performed in LS-DYNA [1] to assess various structural schemes. Design options where the conservatory is fixed to and isolated from the towers have been compared and their impact on building cost has also been provisionally considered.

Different seismic isolator solutions modeled using **MAT_SEISMIC_ISOLATOR* have been envisaged.

This paper presents the modeling methodology and the outcome of the design studies.

Keywords: LS-DYNA performance-based design, seismic isolation, friction pendulum bearing, lead rubber bearing

Figure 1. Raffles City Chongqing – Courtesy of Safdie Architects

Introduction

Arup is a world leader in the application of performance-based design techniques. Validated performance-based approaches combined with advanced simulation have been instrumental to the design of safe, economic and sustainable new buildings.

For over 20 years, Arup has been able to deliver superior seismic performance on particular civil projects by implementing innovative isolator and viscous damper solutions.

For complex nonlinear time-history analysis and performance-based assessments, LS-DYNA has been the software of choice for Arup since 1985 and Arup has worked in conjunction with LSTC to develop a number of specific features for seismic analysis.

Typical in-house applications include soil-foundation interaction, the response of reinforced concrete structural components to seismic loading and the simulation other complex dynamic events.

At present, Arup Shanghai is routinely carrying out 3D nonlinear time-history analysis in LS-DYNA as a validation step for all its special high rise building projects in China.

Raffles City Chongqing

The super-scale development of Raffles City in Chongqing, for which Arup has been appointed to provide structural engineering services for all design stages, will become a new landmark for the city. Located at the heart of Chongqing, at the junction between the Yangtze and Jialing rivers, the site is charged with historic and symbolic significance.

The super-scale development design by internationally acclaimed architect Moshe Safdie is inspired by images of great Chinese sailing vessels on the river. It will pay tribute to Chongqing's noble past as a trading centre and also serves as a symbol of the city thriving present and promising future.

The complex will comprise a shopping mall and eight towers for residential, office, serviced apartment and hotel use yielding a total of GFA exceeding 1.1 million square meters. The development will also serve as a major transportation hub integrating bus, ferry terminals and subway station. Six slender towers will sit atop of a five-storey retail podium; 'gently arching towards the water, they will form the apex to the city peninsula – like the great masts of a ship, with its sails pulling the city forward'[8].

A 400-meter long, glass clad conservatory that bridges the four interior towers at the 60-storey level providing various amenities, green space and 360-degree views of both rivers, is a key architectural element. Its design presents particular engineering challenges.

At concept stage, multiple articulation options for the conservatory bridge needed to be assessed with regard to performance under seismic events and wind loading. A three-dimensional LS-DYNA model of the four supporting towers and the conservatory was developed to capture the dynamic interactions during seismic excitation. The results from these analyses were used for option evaluation and design purpose.

Analysis in LS-DYNA

Analysis objectives

Partial or full isolation of the conservatory bridge are susceptible to offer significant design benefits, in particular:

- Reduce seismic forces in the bridge trusses leading to potential steel tonnage and construction savings
- Reduce the shear forces at the towers/conservatory interface leading to a simplified and cheaper design
- Simplify construction sequence
- Reduce any repair cost on the conservatory after a seismic event
- Meet stringent architectural requirements by allowing a continuous conservatory glass cladding and improving the aesthetics of the observation bridge
- Facilitate thermal expansion

These potential savings and benefits should offset higher bearing cost and MEP complications in the articulation zone between towers and conservatory.

Analysis process

The seismic response of the four supporting towers and the conservatory bridge structure to the strong motion earthquake excitation is simulated by the nonlinear response time-history analysis method in LS-DYNA (971 R6.1.0). Maximum seismic force and displacement demands during the entire seismic events are to be compared with the structure's and bearings' capacities on a component-by-component basis.

The following aspects of the seismic response are considered:

- Structural properties of the concept design of the towers and conservatory
- Mass inertia effects arising from the following sources:
    1- Self weight of all structural components
    2- Superimposed dead loads applied on the tower floors and conservatory deck
- Displacements at the conservatory/tower interface, forces and displacements of the bearings, viscous dampers, etc.

Ground motion excitation

A project specific acceleration response spectrum, corresponding to the Level 3 Maximum Considered Event (MCE) has been provided to the design team. Seven sets (5 natural and 2 artificial records) of spectrum-compatible ground motion time-histories have been derived by the Chinese Expert and prescribed for nonlinear transient analysis. These represent the motions to be applied to the foundations of the towers.

Figures 2, 3, 4 and 5 below show examples of natural ground motion accelerations and their compatibility with the Design Spectrum.

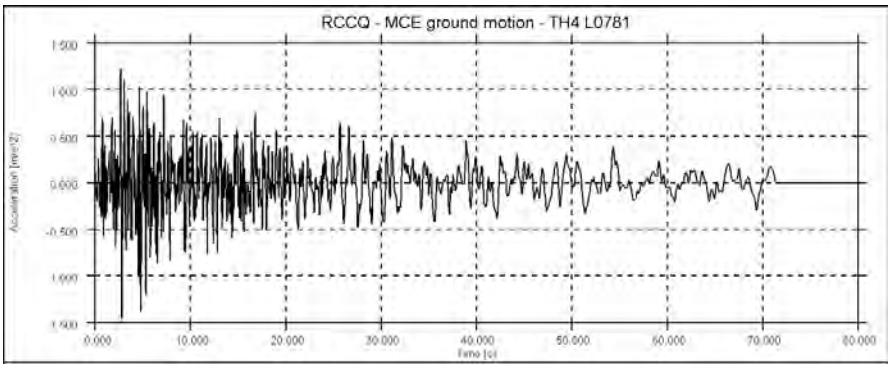

Figure 2. Natural Set 4 (L0781) – Accelerations in E-W direction

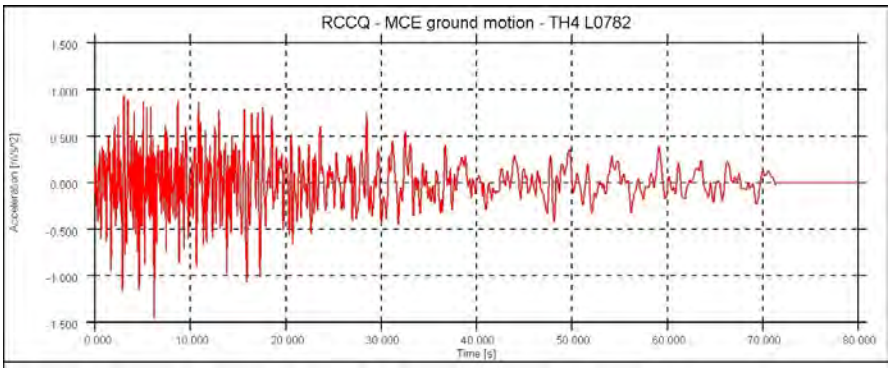

Figure 3. Natural Set 4 (L0782) – Accelerations in N-S direction

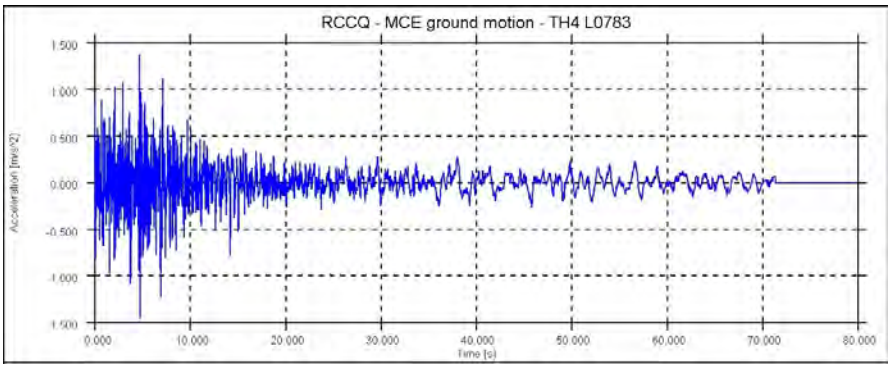

Figure 4. Natural Set 4 (L0783) – Accelerations in vertical direction

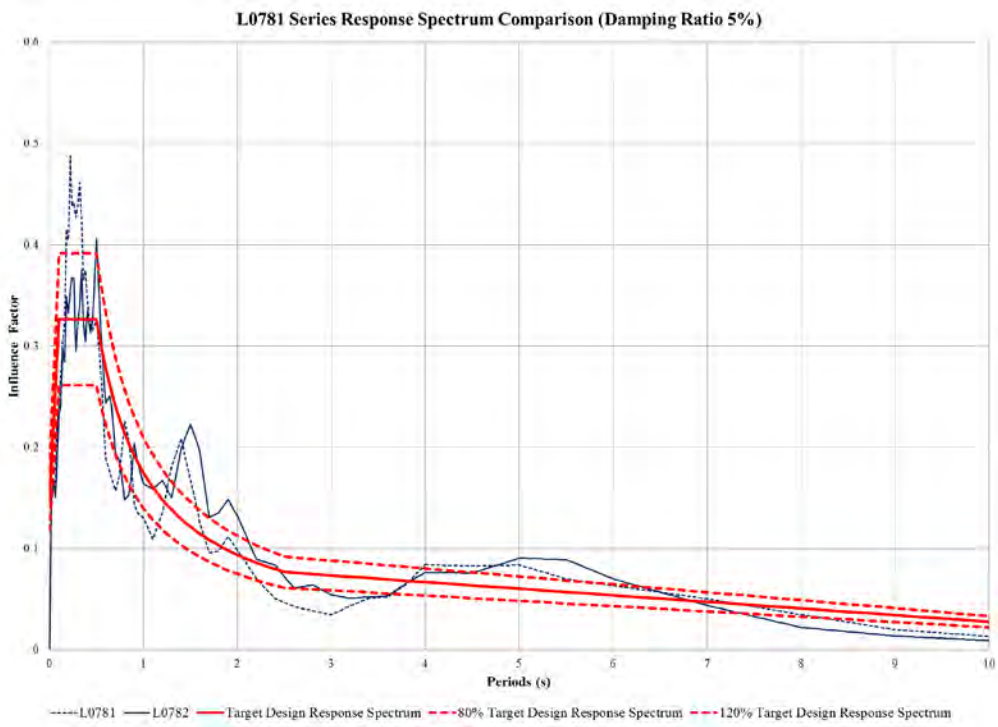

Figure 5: Natural Set 4 (L0781/L0782) – Compatibility with Design Spectrum

Description of the nonlinear analysis model

The tower and conservatory geometry was converted from ETABS and GSA nodal data, elastic sections and material properties, following a methodology used by Arup on various bridges and high-rise building simulation projects.

As part of the validation process, tower and conservatory sub-models were verified against their ETABS/GSA counterparts. Total mass, mass distribution, first natural mode shapes and frequencies proved to compare very well.

One global model consisting of the four T2 to T5 towers and the conservatory structure was assembled and used for the nonlinear seismic response analysis.

Seismic isolation of the conservatory bridge can be achieved by means of elastomeric or sliding bearings. At concept stage, Friction Pendulum Bearings (FPB) and Lead Rubber Bearings (LRB) have been considered.

Realistic modeling parameters and provisional cost estimates have been obtained from established US suppliers: EPS [5] and DIS [6] for FPB and LRB solutions respectively.

Figures 6 and 7 below illustrate typical FPB and LRB designs. For more details on the principle and construction of these seismic isolators, please refer to [5] and [6].

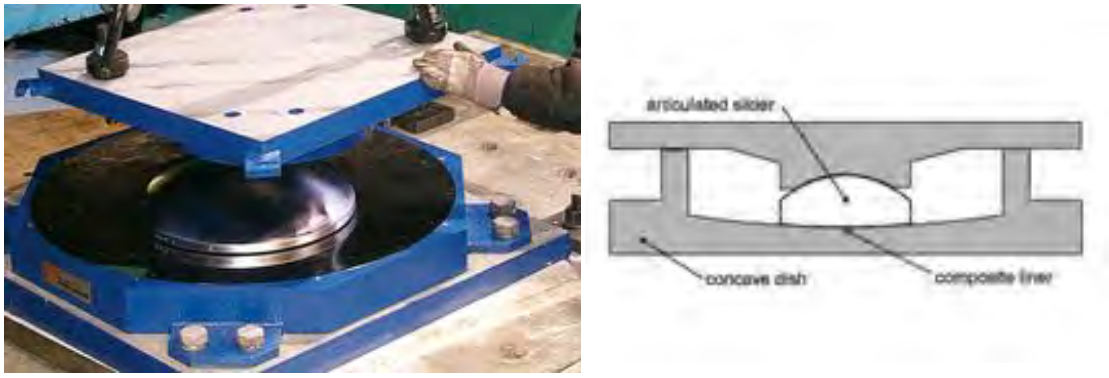

Figure 6. Friction Pendulum Bearing – Courtesy of Maurer Soehne GmbH & Co.

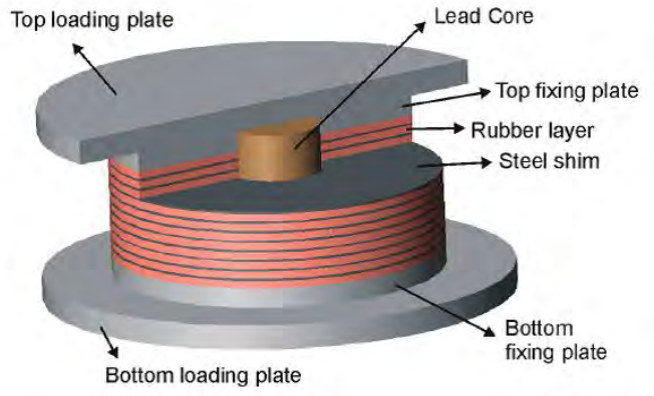

Figure 7. Lead Rubber Bearing

Table 1 below summarizes the range of parameters that have been analyzed.

Bearing type	Design parameters	Values
LRB	Configuration	6 no. per tower – Axial load capacity 33.4MN
	Yielded stiffness	7.2kN/mm
	Characteristic strength	1,025kN
FBP	Configuration	4 no. per tower
	Curvature radius	8m
	Static friction coefficient	3 and 10%

Table 1. Analysis parameters – FPB and LRB options

The **MAT_SEISMIC_ISOLATOR* material is particularly well-suited in LS-DYNA to model the nonlinear force-displacement hysteretic behavior of the isolator bearings. This nonlinear material is formulated using a bi-directional coupled plasticity model with Bouc-Wen smoothing. The hysteretic behaviour was proposed by Wen and Park [2], Wen and Ang [3] and the sliding behaviour was recommended by Zayas and Low [4]. Some additional information about this material is also provided in the LS-DYNA user's manual [1].

Options combining FPBs and viscous dampers have also been considered. The main contribution of the viscous dampers, apart from increasing the damping, is to reduce the displacements at the conservatory/tower interface in both longitudinal and transverse directions.

The viscous damper characteristics used at the concept stage are described below:

Constitutive law is $F=CV^{\alpha}$ with $\alpha=0.3$

Where F: Force [N]

V: Velocity [m/s]

C: Constant

Two values of C have been considered:

Damper type	Constant C	Force at 0.2m/s
Type A	1944788	1.2MN
Type B	4861970	3.0MN

Table 2. Viscous damper properties

Figure 8 gives an example of F=f(V) characteristics

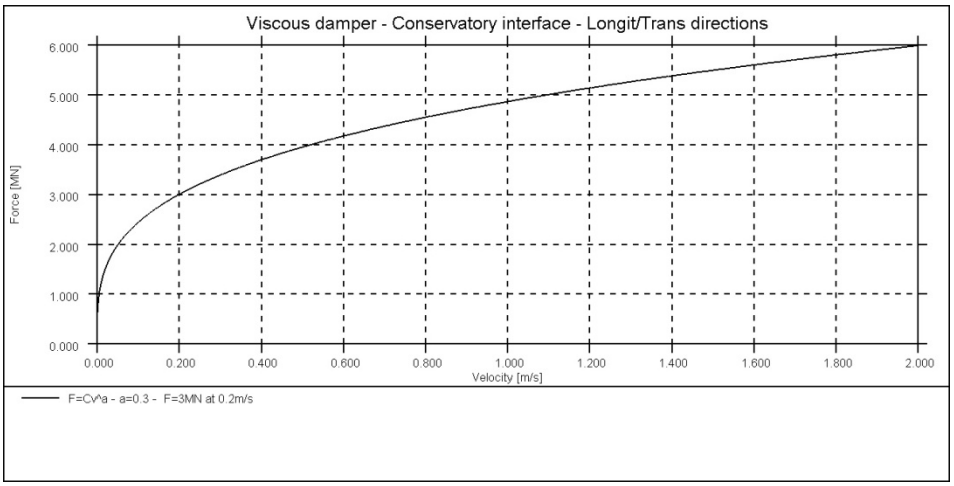

Figure 8. Viscous damper at conservatory interface – Force-velocity characteristics

Modal damping corresponding to 5% of critical has been applied to the analysis model. The first 80 to 85 structural modes depending on articulation option have been considered in order to cover 90% of modal mass and define the frequency range of interest, up to 3.8Hz. The mathematical formulation of modal damping is given in equation (12-56c), Dynamics of Structures by Clough and Penzien [7].

Modes having a modal frequency greater than 3.8Hz are not damped by the modal damping formulation. In order to avoid undesired amplification of undamped modal responses, a Rayleigh damping method is used to treat modes above the main frequency range of interest.

Figures 9 and 10 reflect the exact geometry and extent of the FE analysis model. Towers, seismic bearings and conservatory structure have been modeled explicitly.

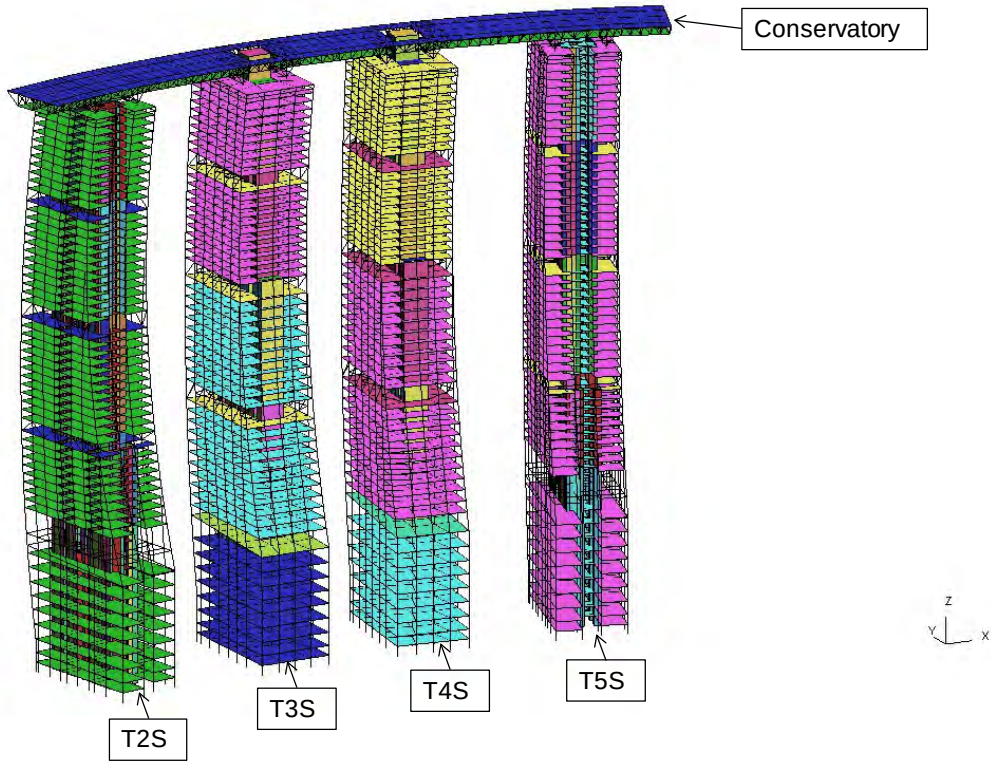

Figure 9. Global LS-DYNA analysis model

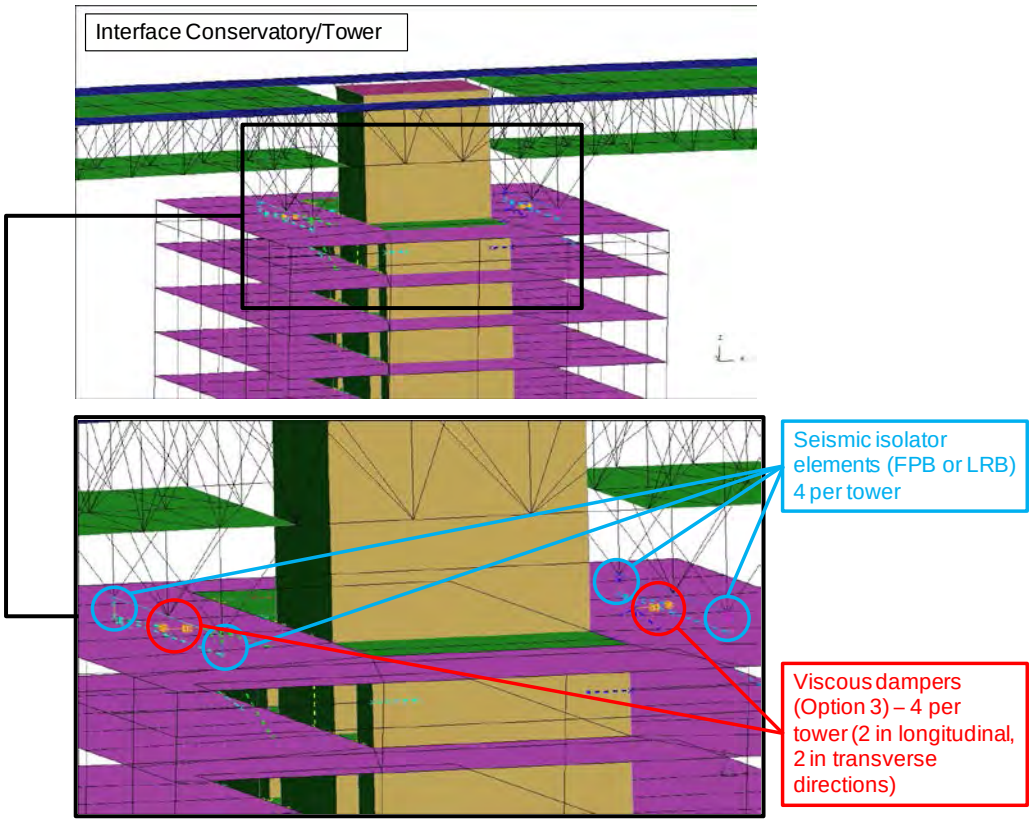

Figure 10. Details of conservatory/tower interface – Isolation cases

Analysis results

A description of the various articulation options tested is given in Table 3:

Articulation option	Description
Option 0	Conservatory not modeled explicitly but conservatory mass distributed at the top of each tower
Option 1	**Conservatory rigidly fixed at all support towers – Baseline case**
Option 2	**Conservatory isolated at all 4 towers**
	2a: 4 no. FPB bearings 3% static friction at each tower
	2b: 4 no. FPB bearings 10% static friction at each tower
	2c: 6 no. LRB bearing at each tower
Option 3	**Conservatory isolated at all 4 towers fitted with viscous dampers**
	3a: 4 no. FPB bearings 3% static friction combined with 4 viscous dampers of type A at each tower
	3b: 4 no. FPB bearings 3% static friction combined with 4 viscous dampers of type B at each tower
Option 4	**Conservatory fixed at T2S and T5S, isolated at T3S and T4S**
	4a: 4 no. FPB bearings 3% static friction at T3S and T4S
	4b: 4 no. FPB bearings 10% static friction at T3S and T4S
Option 5	**Conservatory fixed at T3S and T4S, isolated at T2S and T5S**
	5a: 4 no. FPB bearings 3% static friction at T2S and T5S
	5b: 4 no. FPB bearings 10% static friction at T2S and T5S

Table 3. Description of analysis cases

Predicted maximum shear forces at the conservatory/tower interface, shear forces at the base of towers, tower roof displacements and isolator displacements averaged over the complete set of excitation ground motion cases are reported in Figures 11, 12, 13, 14 respectively.

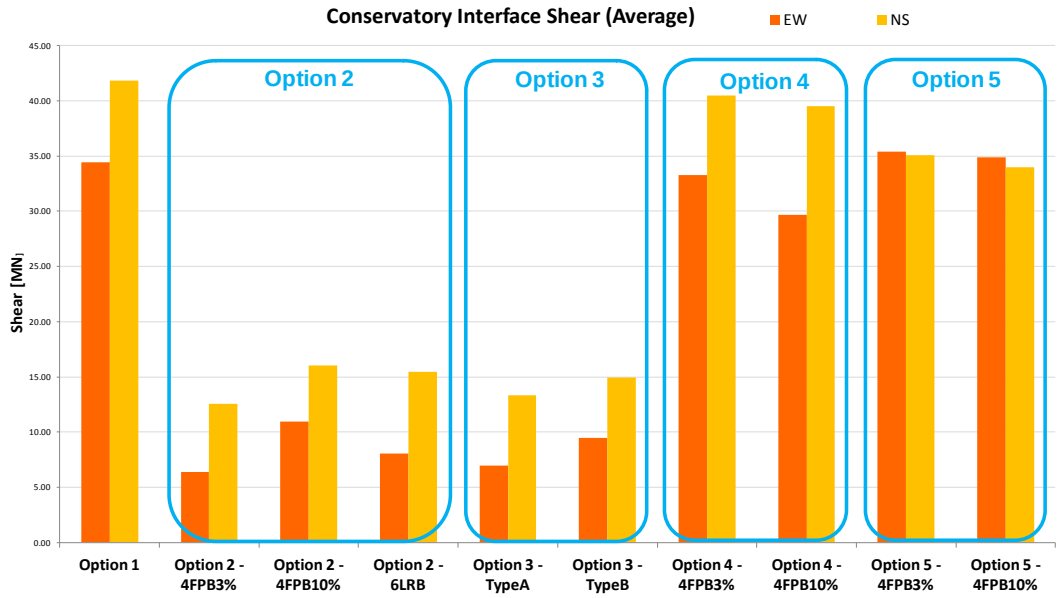

Figure 11. Shear forces at the conservatory/tower interface

For Options 2 and 3, where the conservatory is isolated at all towers, reduction of maximum shear forces at the interface may exceed 65% in both longitudinal (E-W) and transverse (N-S) direction enabling significant material savings and design simplification of the supporting structure at the top of the towers. For Options 4 and 5, the benefits are much more marginal with a reduction in maximum shear force in the order of 5-15%.

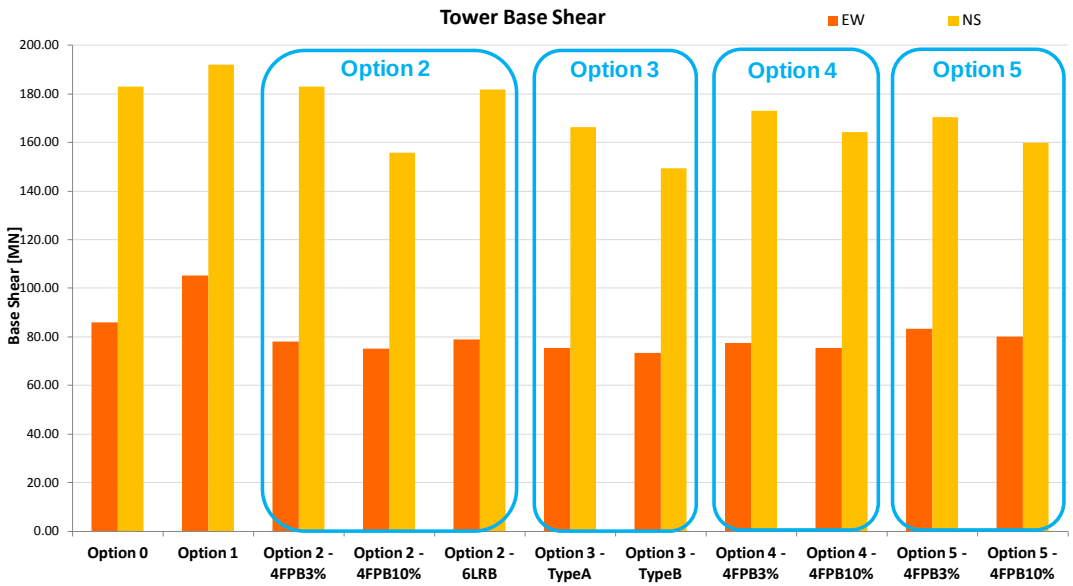

Figure 12. Shear forces at the tower bases

All isolation options are beneficial in terms of reduction of shear forces measured at the base of the towers. In the best case (Option 3 – Type B), this reduction can reach 30% compared to the fixed conservatory option.

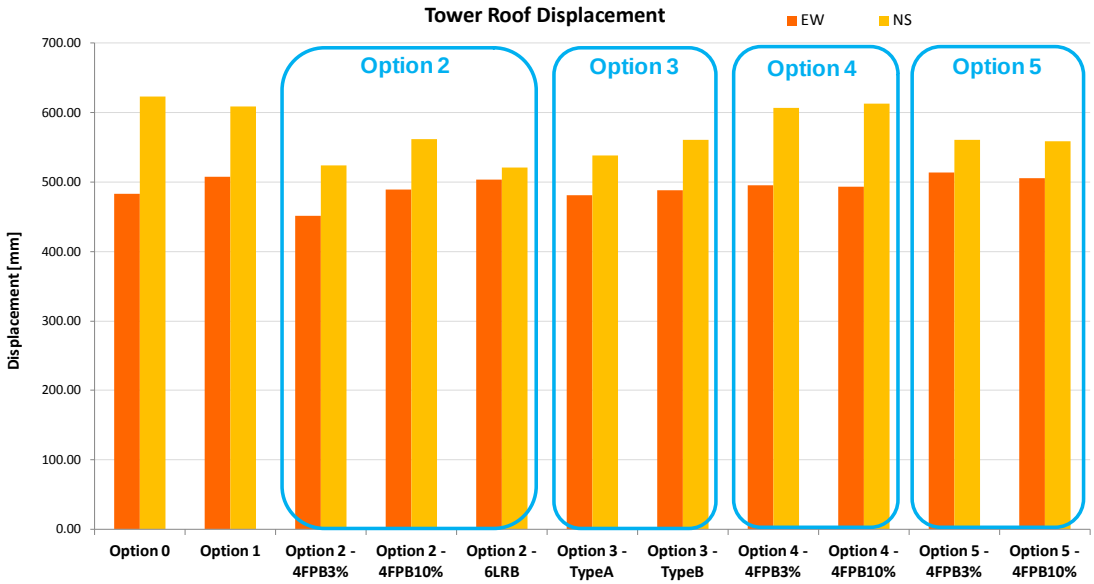

Figure 13. Tower roof displacements

Options 2 and 3 again offer some limited reduction of maximum displacements at the top of towers in both directions. This displacement reductions range between 4 and 14% compared with the baseline fixed conservatory model.

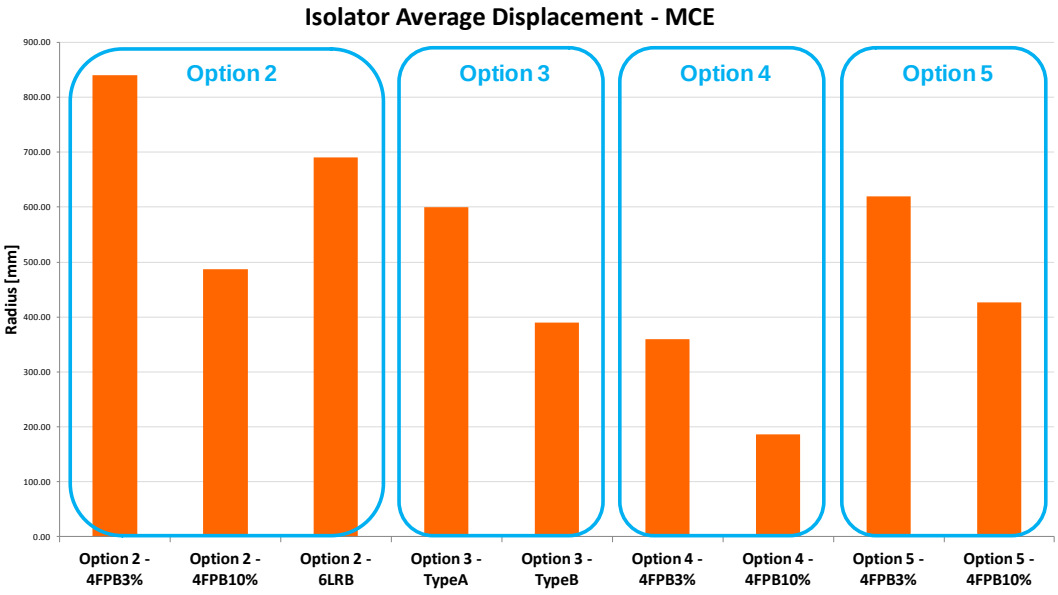

Figure 14. Isolator displacement demands

Given that a design safety factor must be applied to the predicted isolator displacement demands, Option 2 – 4FPB3% is likely to require FPB diameters in excess of 2 meters and therefore to have negative practical and cost implications.

For the fixed conservatory design and the articulation options considered, a first schematic optimization of the conservatory truss structure to meet Level 3 MCE design requirements has been performed. Figure 15 below summarizes potential steel tonnage savings for some isolated schemes.

Assuming a cost of steel in China of 15k RMB/ton including fabrication, erection and fire-proofing, potential savings on the conservatory primary truss amount to 2-3m RMB.

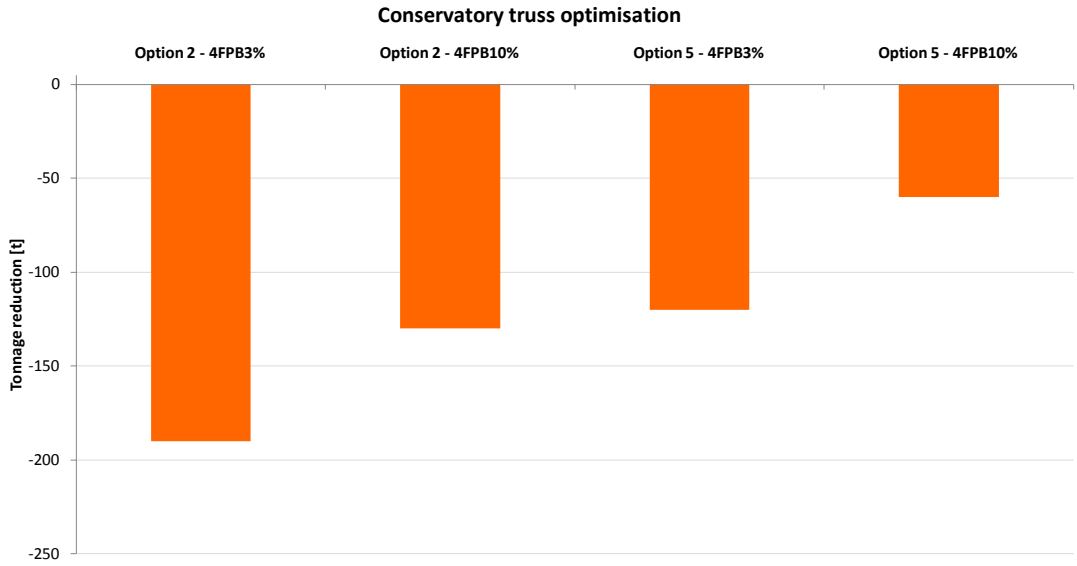

Figure 15. Conservatory steel tonnage reduction

Conclusions

Using advanced LS-DYNA features to simulate seismic isolators, various conservatory articulation schemes could be assessed and viable solutions identified at an early design stage.

Based on the cost estimates provided by EPS and DIS and considering the potential steel tonnage under Option 3, the use of viscous dampers combined with seismic isolators seems prohibitive. The most cost effective solution appears to be Option 2 (seismic isolators at all towers) either with FPB 10% static friction coefficient or Lead Rubber Bearings.

Next steps

Option 1 (Fixed conservatory) and Option 2 (4FPB10% or LRBs) will continue to be reviewed as the models of the towers and conservatory are being modified and refined in the next project phases.

In particular, the nonlinear behavior of the structure and the damage extent in key components will be represented more accurately as the design scheme is being fixed. Some of these detailed analyses will also be performed in LS-DYNA. The assessment outcomes of the articulation options and the selected solution will be presented to and discussed with both Client and Chinese Expert Panel.

References

[1] LS-DYNA® Keyword User's Manual, Version 971. Livermore Software Technology Corporation (LSTC): Livermore, CA 94551-5110, USA, May 2007

[2] Wen, Y.K., "Method for random vibration of Hysteretic Systems", Journal of the Engineering Mechanics Division, ASCE, Vol. 102, No. EM2, 1976.

[3] Park, Y. J., Wen, Y.K. and Ang, A. H-S., "Random vibration of hysteretic systems under Bi-Directional Ground Motions" Earthquake Engineering and Structural Dynamics, Vol. 14, 1986.

[4] Zayas, V. and Low, S., "A Simple Pendulum Technique for Achieving Seismic Isolation" Earthquake Spectra, Vol. 6, No. 2, 1990.

[5] Earthquake Protection Systems, Inc (EPS). www.earthquakeprotection.com

[6] Dynamic Isolation Systems, Inc (DIS). www.dis-inc.com

[7] R.W. Clough and J. Penzien. Dynamics of Structures, 2nd Edition, McGraw-Hill, 1993

[8] http://www.msafdie.com/file/4218.pdf

Application of CPM in Simulating the Deployment of IC

Rong Zhang[1], Qiang Liu[2], Luther Ma

（Autoliv (Shanghai) Vehicle Safety System Technical Center Co.,Ltd.
1000 Beihe Road, Jiading, Shanghai, 20187, China）

Abstract: This paper introduces the implementation of CPM in simulating the deployment process of IC. We first use CPM to simulate the mass flow of gas particles in the airbag, and then use CPM Sensors to determine the gas pressure at specified points. The simulation results show a good consistent with the test data. It must be noted that, in addition to correctly using CPM, a good simulation results also results from an appropriate setting of contact parameters and a correct use of MAT34. Several important aspects in developing an IC model, such as fold methods, contact setups, material parameters, CPM setups and comparison with experiments, are included in this paper. The paper finally shows that CPM is a promising method which is able to remarkably reduce the cost for designing airbags.

Keywords: CPM, IC, gas pressure, static deployment

1 Introduction

Airbags are widely used in the passive safety system of an automobile and play an important role in the modern automobile industry. At the stage of early design, each modification imposed on the airbag should be verified by a static deployment test to see whether the initial goal of this modification is achieved or not. As a result, when a certain type of airbag is ready to be manufactured, a huge number of deployment tests had already been conducted. In view of this, a cost-saving way for designing an airbag may be attributed to the possibility of reducing the number of deployment tests by CAE simulation.

Recently, a new feature known as ‘Corpuscular Particle Method’ (CPM in abbreviated) or *AIRBAG_PARTICALE in LS-DYNA has been included in LS-DYNA. In contrast to other existing methods, CPM focuses on the real natural of deployment, i.e. the mass flow of gas in the airbag; hence, the result derived from this method is more accurate and reliable. Consequently, simulating the deployment of an airbag using CPM in LS-DYNA instead of the real deployment tests is an efficient and cost-saving way for designing airbags. This paper introduces how to simulate the static deployment of IC by using corpuscular particle method.

[1] Email address: rong.zhang@autoliv.com
[2] Email address: Qiang.liu@autoliv.com

2 Fold model of IC

Due to the limitation of space in a vehicle, all types of airbags (including DAB, PAB KAB and IC, etc.) are located in specified positions. Different locations and different fold methods will give rise to various postures of an airbag at deployment.

2.1 Meshing and reference meshed model

One of the most popular fold methods for IC is convoluting the cushion along a certain axis parallel to the in-vehicle direction. The mesh is required to be regularly distributed along the convolution direction so as to reduce penetration. Note that the element size should be carefully chosen. An IC with large element size will degrade the quality of the finite element model, whereas a very small element size will significantly increase the time-cost of calculation. Generally speaking, an element size of 8 mm is suitable for most cases. Refining the topology of the mesh according to the real structure and then seaming all cushions to form a closed cavity, we finally obtain the finite element model of IC as shown in Figure 1.

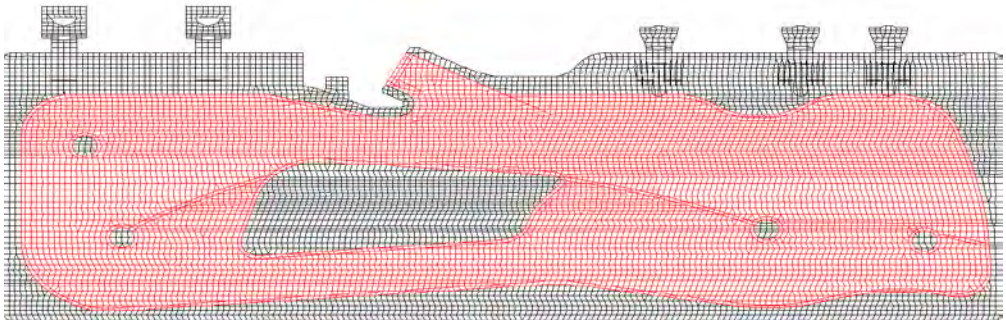

Figure 1. Meshed model before folding

As long as the element size are modified appropriately, all nodes are then exported to a reference meshed model via the card *AIR_FRFERENCE_NODES. This reference meshed model is used as the reference which ensures every element keeps its shape undistorted before and after folding, and further ensures the total volume of IC keeps constant.

2.1 Fold method

There exist various fold methods for IC. Two commonly used methods may be attributed to the ‘inboard’ and ‘outboard’ methods (see Figure 2). Other methods derived from these two basic methods are also adopted in the real practice, e.g. the method called ‘inboard + 1’. Generally speaking, the deployment speed of an IC which uses the inboard fold method is much faster than that using the outboard method. However, it is found that the outboard method can achieve a more efficient protection than its inboard counterpart. This paper focuses on outboard-folded IC only.

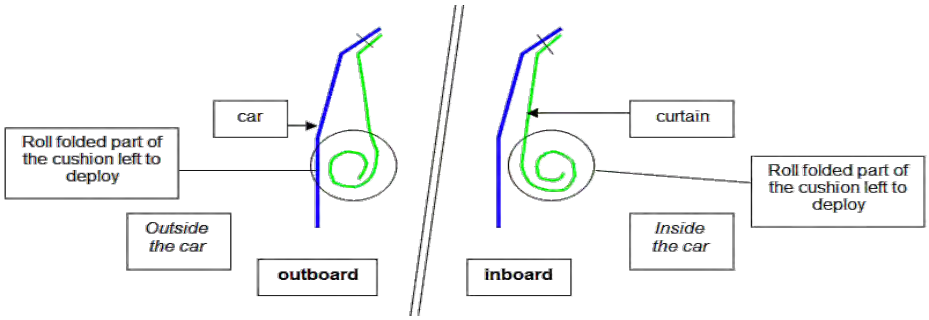

Figure 2. Outboard and inboard fold methods

DYNA provides several methods and tools for folding an IC. In this paper, we choose the folding procedure as follows: (1) fold the IC by DYNA's fold tool, (2) setup an dynamic analysis to insert the inflator into the cushion, and (3) fix the IC (with inflator) to the right place through five brackets.

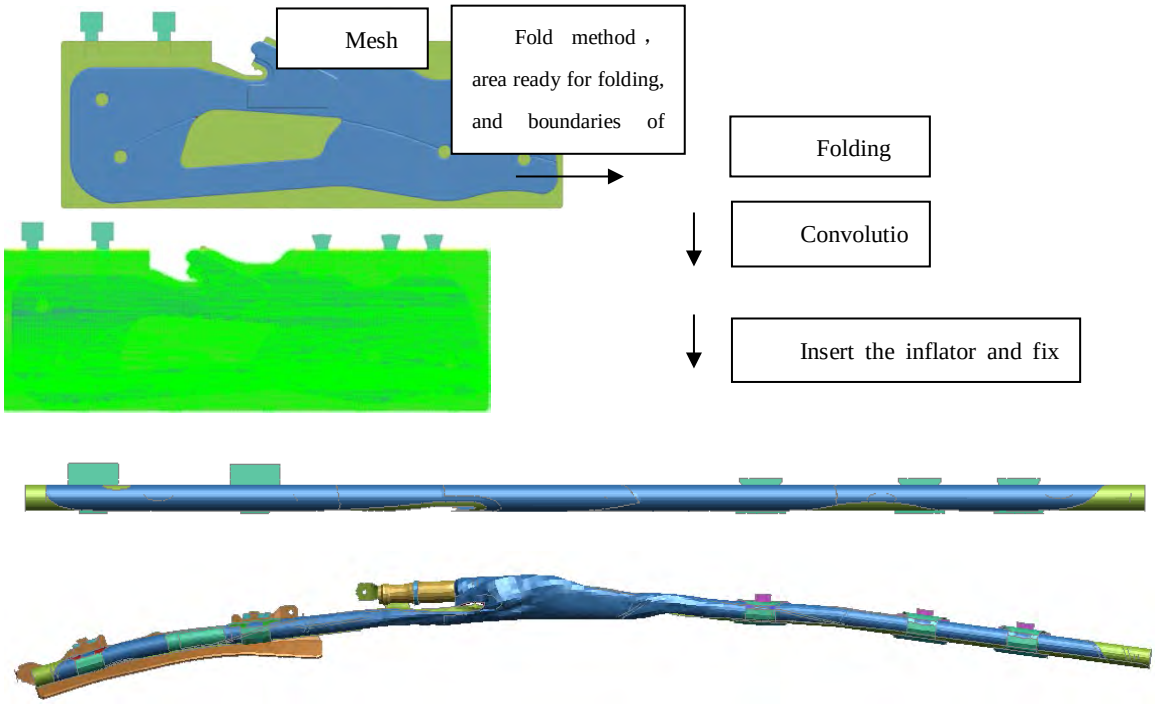

Figure 3. Procedure of folding and fixing an IC

3 Contact and boundary conditions

The finite element model is constructed on the basis of experimental setups, as shown in Figure 4. The model includes three types of contact: (1) self-contact in all parts of IC (including the inflator), (2) the contact between the IC and its surrounding parts, and (3) the self-contact in all IC's surrounding parts.

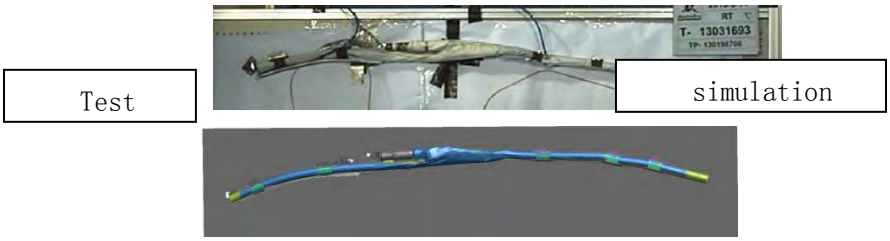

Figure 4. Experimental set-up and finite element model

(1) Self-contact in IC: *CONTACT_AIRBAG_SINGLE_SURFACE_ID. Note that, since the material used for cushion is very soft, a set of contact parameters with appropriate values should be well defined so as to avoid penetration;

(2) Contact between IC and surrounding parts: This type of contact can be defined via the card *CONTACT_AUTOMATIC_SURFACE_TO_SURFACE_ID;

(3) Self-contact in IC's surrounding parts: This type of contact can be defined via the card * CONTACT_AUTOMATIC_SINGLE_SURFACE_ID;

Table 1 shows the recommended parameter values for the three types of contacts discussed above. Here we must emphasize that the boundary conditions of the finite element model are required to be consistent with the experimental setup as well as the way that the IC is connected to the fixture. Moreover, the input parameters for gas should be set according to the type of inflator and modified by the use of Tank test model.

	Parameter	SFS	SOFT	SBOPT	DEPTH
Self-contact in IC	Recommended Parameter values	>1	2	3	5
Contact between IC and surrounding parts		0	2	3	5
Self-contact in IC's surrounding parts		0	1	0	0
Note: Parameter values showing above may vary for different cases					

Table 1. Recommended parameter values for the three types of contacts

4 Material parameters

The model consists of both metal materials and fabric materials. Material materials is defined via the material card MAT24; the fabric materials for cushion are defined through the card *MAT_FABRIC_TITLE with the parameter values shown in Figure 5.

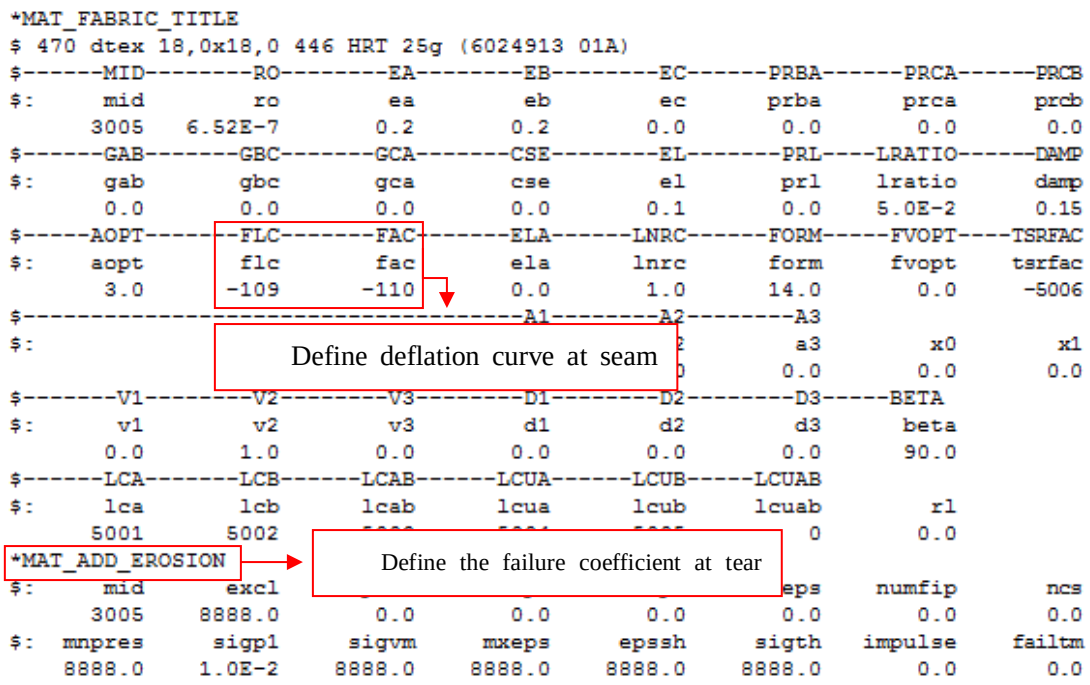

Figure 5. Material parameter of the fabric material for cushion

It must be noted that:

(a) Since IC will deflate through the seam lines, deflating parameters are required to be assigned to the material at these regions (via the curve flc\fac);

(b) The tear lines are defined by using the keywords *MAT_ADD_EROSION. Note that the failure time much be coincide with the real data;

(c) Setting CSE=1 or 0 will affect both the deployment speed and the distortion of element. In general, setting CSE=1 accelerates the deployment speed and, at the meaning time, elevates the shrinkage of an element. For detailed explanation the interested reader may refer to DYNA's user manual.

5 Setting of CPM

In essential, CPM simulates the gas generated by the inflator by using a large number of particles, whose properties are defined in the card *AIRBAG_PARTICLE_ID according to the type of inflator (see Figure 6). Here (1) SID1 specifies the parts which contacts with the gas directly, (2) SID2 defines the internal parts inside the cavity given in SID1, (3) several parameters prescribe the characteristics of the gas, and (4) the remaining parameter are used as the control parameters for the mass flow. By virtue of these parameters, the posture of IC at deployment shows a good consistent with the real case observed by experiments. That is why CPM is more advantage than other existing methods.

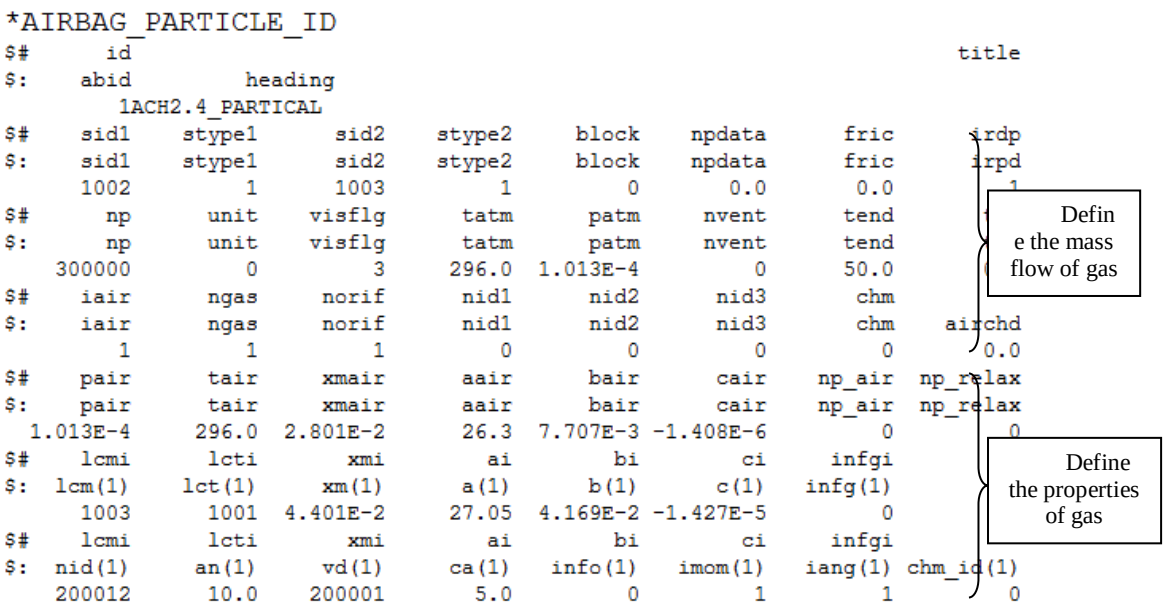

Figure 6 Setup of AIRBAG_PARTICAL

For now, CPM is unable to measure the basic information (e.g. the gas pressure) at a specified point in the mass flow. In other words, CPM does not focus on one particle, but is based on the mean average of a bunch of particles. To solve this problem, DYNA includes a new card *DATABAES_CPM_SENSOR to detect the averaging velocity and the total mass of the particles in a certain region at any instant of time, and then determines the variation of the gas pressure with time by using the theory of idea gas. Generally, we place the CPM Sensor at the same location where we place the pressure sensor in the real deployment test.

6 Results and comparison with experiment

From Figure 7 it can be found that the postures of IC derived from simulation matches the test video very well. Figure 8 compares the gas pressures measured by CPM Sensors with those measured by the pressure sensors in the experiment. From the figure one can see that the simulation result is in a good agreement with the experimental data, indicating that CPM Sensor is able to detect the gas pressure with a reliable accuracy.

7 Conclusion

Corpuscular particle method (CPM) simulates the mass flow of gas particles in an airbag during the process of deployment, by using of which the gas pressure as well as the posture of the airbag at any instant of time are determined. Since CPM focuses on the real nature of the movement of an idea gas, the simulation results are more accurate than those derived from other existing methods. Consequently, CPM is a promising method which can remarkably reduce the cost for designing an airbag.

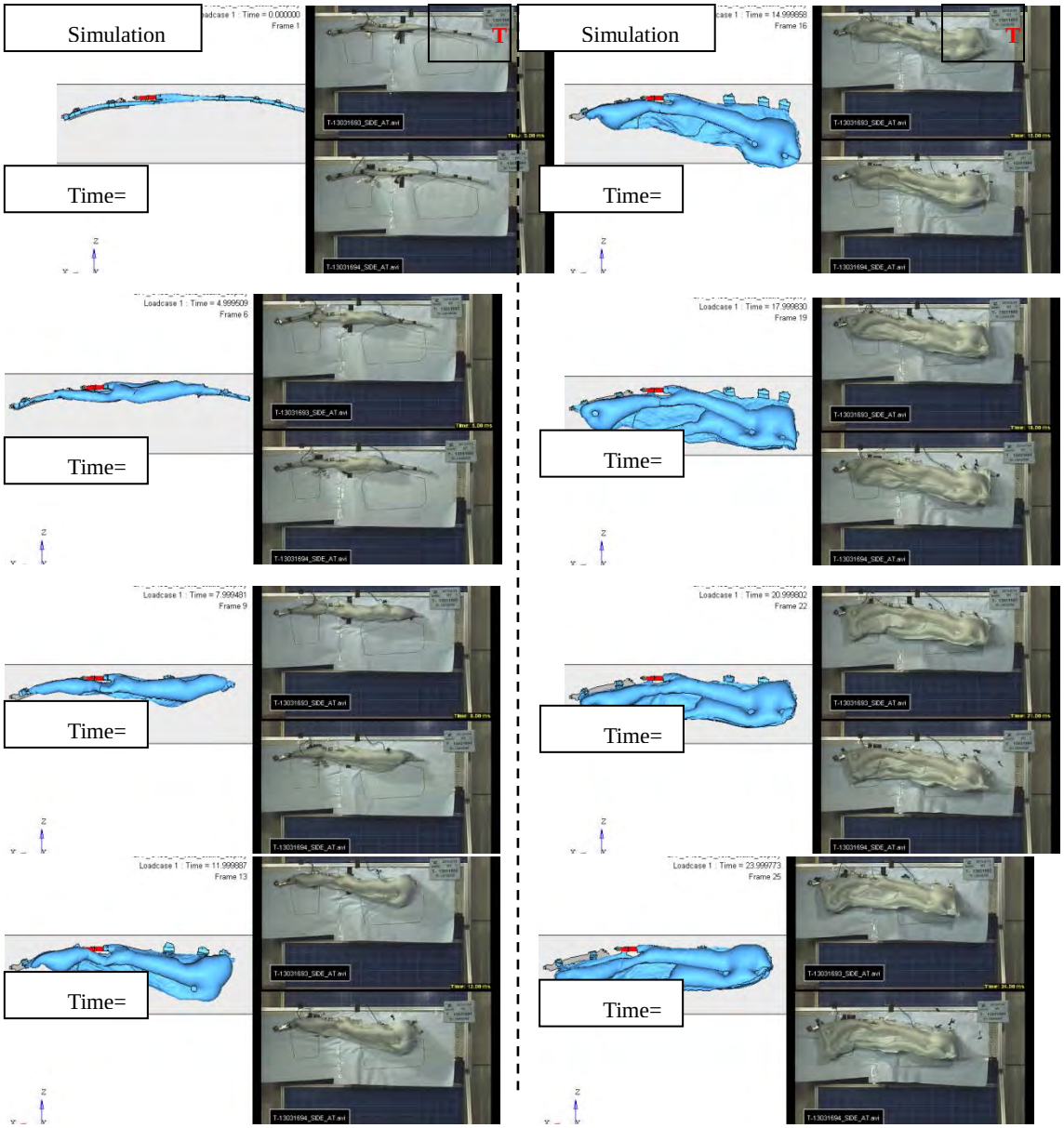

Figure 7 Comparison of simulation results with test video

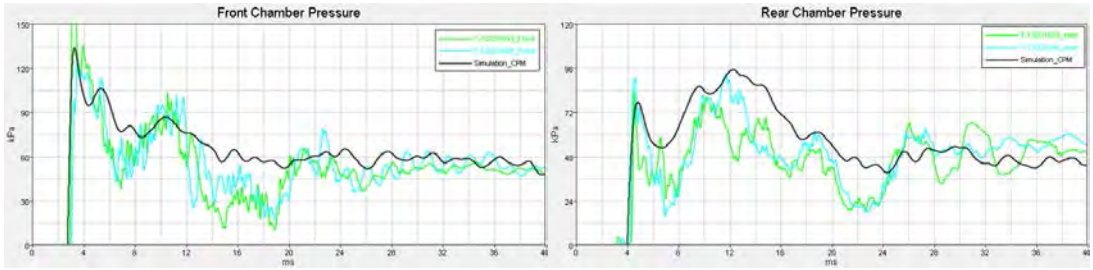

Figure 7 Comparison of the gas pressure derived from CPM Sensor with the experimental data

Assessment of Simplified Numerical Models for Vehicle-bridge Dynamic Interaction

Juan WANG，Jiang QIAN

（State Key Laboratory of Disaster Reduction in Civil Engineering, Tongji University, Shanghai, 200092, CHINA. daphnei@163.com）

Abstract： The main objective of the presented study is to review and evaluate simplified finite element (FE) models used for dynamic vehicle bridge interaction studies. The considered simplified models have been developed using new features implemented in LS-DYNA for computer simulation of moving loads. This new modeling approach offers a balance between computational efficiency and accuracy, and is especially useful for extensive parametric studies on dynamic response of bridges induced by traffic loading. Models for a simply supported beam subjected to a moving mass and one-axle vehicle with spring and damper respectively are used to verify the corresponding FE algorithm through comparison between FE results and existing analytical or semi-analytical solution obtained from MATLAB procedure. In addition, a more complex FE model for a girder-slab-barrier bridge coupled with a heavy truck is developed based on experimental data. After validation of FE models, sensitivity of dynamic amplification factor (DAF) to vehicular parameters including velocity, weight ratio of vehicle over the bridge, and damping of the vehicle is investigated. DAF was found to be generally ascending with growing velocities and local peaks occurring at certain velocities.

Keywords： dynamic amplification factor; finite element model; LS-DYNA; vehicle bridge interaction; verification and validation

The main objective of the presented study is to develop simplified yet efficient numerical models for vehicle-bridge systems. Such models should present a good balance between efficiency and accuracy. Three types of numerical models were developed based on LS-DYNA commercial code to represent bridge and truck interaction system. Two simple models of simply supported beams subjected to a moving mass and a one-axle vehicle respectively are used to verify the efficiency and reliability of the FE algorithm. Subsequently, in order to keep a good balance between simplicity of the FE models and computational accuracy, the FE models of bridge and heavy truck are developed based on availability of experimental data. Moving velocity, weight ratio of a truck over a bridge are selected for parametric study after verification of FE models.

In the following section, DAF, defined as maximum dynamic displacement of structure resulted from moving loads over maximum static displacement, is used (Brady et al. 2006).

1 A simply supported beam subjected to a single moving mass

1.1 Simple FE model

The easiest model for vehicle and bridge interaction system may be given by a simply supported beam subjected to a single moving mass which represents the idealized vehicle as shown in Fig. 1. For brevity, the following dimensionless variables are adopted: $\alpha=\pi v/(l\omega_1)$, $\beta=\omega_d/\omega_1$, $\tau = vt/l$, where v - constant velocity; l - length of span; ω_1 - the first natural circular frequency of the beam; ω_d - circular frequency of damping of the beam. The analytical solution of is offered by Fryba (1999).

A simple vehicle model was developed taking advantage of new features included in the FE code LS-DYNA. These features is defined by two cards (*RAIL_TRACK and *RAIL_TRAIN) developed by Arup (Hallquist 2013) to represent wheel-rail contact. RAIL_TRAIN keyword defines contact patch between wheel and rail. RAIL_TRACK keyword specifies tracks followed by wheels. Here a simply supported beam is modeled using shell elements. The moving mass is represented by a one-node mass element.

1.2 Validation

The beam is 6 m long with the elastic modulus of 210 GPa, the rectangular cross section of 0.2 m by 0.12 m, and the density of 7.85 103 kg/m3. These properties result in the beam having natural frequencies of 13.01Hz, 51.88 Hz, 116.05 Hz, 204.66 Hz, and 316.56 Hz by FE analysis. The corresponding analytical results are 13.03 Hz, 52.12 Hz, 117.27 Hz, 208.47 Hz, and 325.74 Hz.

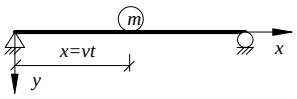

Fig. 1. A simply supported beam subjected to a moving mass

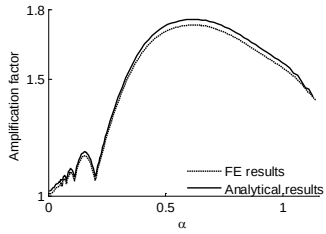

Fig. 3. An effect of velocity on amplification factor between FE and analytical results without damping

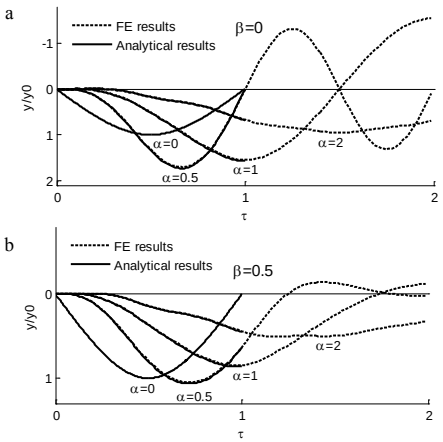

Fig. 2. Dynamic displacement at mid-span for different velocities and damping parameters: a- β=0; b- β=0.5

To further verify numerical models, time histories of vertical displacement at the midspan of the beam is shown in Fig. 2 where dimensionless displacement, dynamic over static displacment at midspan, is adopted. Fig. 3 displays DAF at a number of velocities. The diagrams indicate that FE results agree well with analytical ones. The results shown in Fig. 3 demonstrate that at least four local maximum values or local peaks exist at dimensionless velocities of α=0.069, 0.095, 0.155, and 0.626, namely subcritical velocities, and these FE results are very close to analytical results which are 0.069, 0.095, 0.155, and 0.610. It is considered that velocity of α = 1, at which the frequency of loading equals to first natural frequency of bridge, is the critical point to trigger resonant response of bridge (Fryba 1999). However, the maximum of DAF does not occur at the point of α=1. The reason is that the vertical displacement is calculated during the time of forced vibration of bridge, namely, $\tau \leq 1$ and the acting time of moving load at high velocity is too short for a beam to respond. For the beam without damping or with light damping, the maximum dynamic response happens at time of

τ>1, i.e. after the moving mass left the beam. The exact subcritical velocities were described by Brady et al. (2006). The first three subcritical velocities in this work are very close to Brady's results which are 0.067, 0.092, and 0.148 while the biggest one is more than that of Brady's which is 0.383. It may be because of different ways to calculate the maximum response which is not revealed in the latter paper.

2 A simply supported beam subjected to one-axle vehicle

2.1 Analytical solution

The vehicle can be represented by one-axle system consisting of sprung mass, m_1, and unsprung mass, m_2, connected by a spring and a damper as shown in Fig. 4. The equations of motion for the bridge-vehicle system are as follows (Fryba 1999)

$$m_1 d^2 y_1(t)/dt^2 + cd[y_1(t) - y(\eta,t)]/dt + k[y_1(t) - y(\eta,t)] = m_1 g \tag{2}$$

$$EJ\partial^4 y(x,t)\partial x^4 + \mu\partial^2 y(x,t)\partial t^2 + 2\mu\omega_d \partial y(x,t)/\partial t =$$

$$\delta(x-\eta)\{m_2 g - m_2 \partial^2 y(x,t)/\partial t^2 + k\left[y_1(t) - y(\eta,t)\right] + cd\left[y_1(t) - y(\eta,t)\right]/dt\} \tag{3}$$

where k and c - the stiffness and damping coefficients; y_1 and y - vertical displacement of the sprung mass and beam; η=vt. Using the modal superposition method, Eqs (2) and (3) can be transformed to a series of ordinary differential equations, and the detailed manipulation was shown by Akin et al. (1989). In this paper, the transformed equations were solved using Newmark β method according to iteration steps stated by Olsson (1985).

2.2 Validation of FE models

The sprung and unsprung masses are represented by one-node mass elements, and spring and damper are modeled by discrete elements. The damping of the spring, c, is 20 000 N s/m; the stiffness of the spring, k, is 1N/m; the masses of m_1 and m_2 are 100 kg and 1 kg respectively. The beam is the same as the previously described before. The comparison of the vertical displacement at midspan and the sprung mass, m_1, between FE results and numerical results are shown in Fig. 5 for velocity of 50 km/h, showing that good match is observed. Effects of velocity on DAF for FE and analytical results are shown in Fig. 6. It displays an ascending trend similar to the previous one-mass model with local maximum for the subcritical velocities 0.064, 0.089, 0.146, and 0.554.

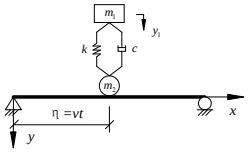

Fig. 4. A simply supported beam subjected to one-axle vehicle

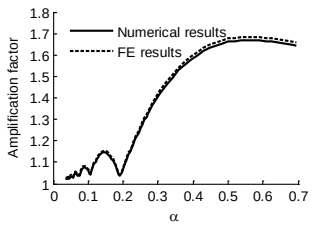

Fig. 6. Effect of velocity on amplification factor between FE and analytical results for one-axle system

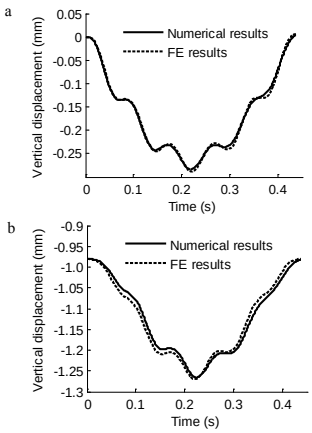

Fig.5. Time history of vertical displacement: a - midspan of the beam; b - the sprung mass, m_1

3 Concrete bridge traveled by a heavy truck

3.1 FE models and validation

Development and validation of FE models of a girder-slab-barrier bridge and a heavy truck were based on available experimental data (Li et al. 2008; Kwasniewski et al. 2006a and 2006b). The tested bridge is built of slab on girder with barriers as shown by Li et al. (2008). The bridge has three spans and two lanes with each span 21.7 m long and 14.15 m wide. The cast-in-place concrete slab, 0.2 m thick, is supported by six AASHTO type-III girders with a spacing of 2.4 m. The barrier and diaphragm are represented by standard beam elements with rectangular section. Discrete beam elements are used to model bearing pads. Girders are simulated by standard beam elements with I shape cross sections. The slab is built of shell elements with composite sandwich material. The determination of sizes of cross section of beams and simplifying implementation are based on the method presented by Kwasniewski (2010). The shell elements are composed of six layers with different material properties for layers of rebar and concrete. The locations for reference planes of beam elements for barrier and girder and diaphragm are determined to comply with the corresponding real structural configuration as shown in Fig. 7. The actual composite components are

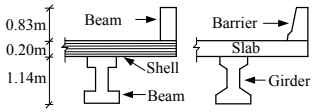

Fig. 7. Bridge numerical simplification (left) and its actual composite configuration (right)

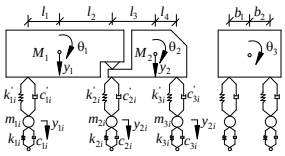

Fig. 8. Analytical model of heavy truck with 11 DOFs

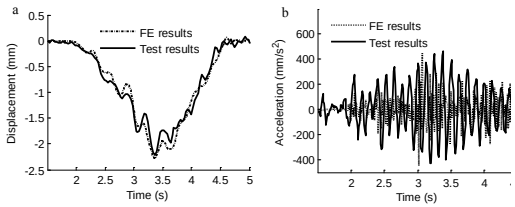

Fig. 10. Comparison of experimental data and FE results at velocity of 48 km/h: a - displacement; b - acceleration

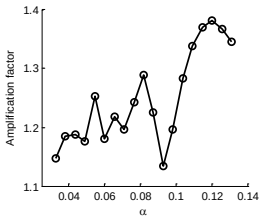

Fig. 12. Calculated amplification factor dependent on velocity

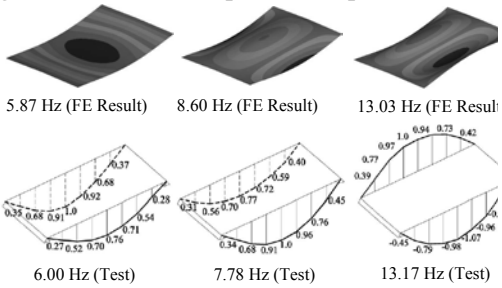

Fig. 9. Comparison of natural vibration modes between field experimental data of bridge (Li *et al*. 2008) and FE analysis.

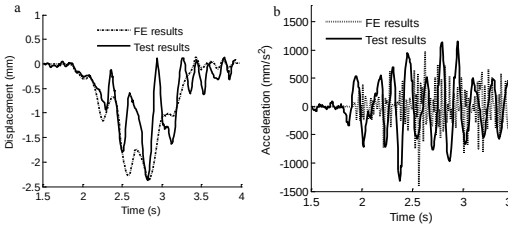

Fig. 11. Comparison of experimental data and FE results at velocity of 80 km/h: a - displacement; b - acceleration

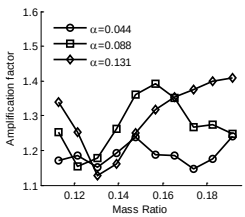

Fig. 13. Calculated amplification factor vs. mass ratio for three selected velocities

considered as linearly elastic. Material properties for girder and slab were determined by testing of concrete core samples (Kwasniewski et al. 2006a). The boundary condition without friction are applied at bearing pads.

A heavy truck is modeled as a three-axle articulated truck with 11 degree of freedom (DOF) as shown in Fig. 8. It is composed of one-node mass elements for wheels, 3D bodies built of solid elements for tractor and trailer, and spring and damper elements for the suspension and tires. The tractor and trailer are assumed to be rigid bodies, connected by a spherical joint. Geometry and dimensions of the truck model were extracted from Li et al. (2008). Mass distribution and stiffness for tires and the suspension system are determined to make each static axle force equal to the actual measurements. The static wheel loads of front, middle, and rear axles are 50 kN, 100 kN, and 169 kN respectively. The total weight of the truck is 319 kN (32.5 Ton). Natural frequency for the whole body bouncing mode is 3.42 Hz.

Three modal shapes and natural frequencies are found to correspond to the experimental results (Li et al. 2008) as shown in Fig. 9. Two cases of dynamic experimental data are selected to verify the integrated FE model. The two cases are for the truck running along the center of roadway at velocity of 48 km/h (30 mph) and 80 km/h (50 mph) without a wood plank (see Kwasniewski et al. 2006a for details). Fig. 10 and 11 show results for the run at 48km/h and 80 km/h respectively. With accepted discrepancy, the presented simplified FE models can be considered sufficient to represent real structure.

3.2 Parametric study

Truck velocities are selected within range from 30 km/h to 120 km/h with increment of 5km/h, corresponding to dimensionless velocity from α=0.033 to 0.131. DAF for various velocities is displayed in Fig. 12. It is visible that there are three local peaks at subcritical velocities of α=0.055, 0.082 and 0.120. It also implies that for three-axle truck the local maximum of DAF occurs at certain velocities. For mass parameter study, additional weight of 25kN is applied for the truck by increasing the mass of the trailer. The corresponding mass ratio of the truck over the bridge ranges from 0.11 to 0.19. The results for velocities of α=0.044 (40 km/h), 0.088 (80 km/h), and 0.131 (120 km/h) are presented in Fig. 13. It shows again that DAF does not necessarily increase monotonously with mass ratio for three-axle vehicle.

4 Conclusions

Three types of numerical models of vehicle-bridge interaction have been considered based on LS-DYNA commercial code. The simple models, consisting of a simply supported beam subjected to a moving mass or one-axle system, have very limited application but can be easily verified through comparison with existing analytical and semi-analytical solution. More complex and accurate model of the bridge and three axle heavy truck was validated using experimental data obtained from full scale tests. Experimental validation shows that the last model represents a good balance between efficiency and accuracy and is well-suited for parametric studies. Presented parametric study indicated the existence of local peaks of DAF. The local peaks of DAF occur at a number of certain dimensionless velocities.

References

[1] Akin, J. E.; Mofid, M., Numerical solution for response of beams with moving mass, Journal of Structural Engineering,1989; 5(1) , 120-31.

[2] Brady, S. P.; OBrien, E. J.; Znidaric, A., Effect of vehicle velocity on the dynamic amplification of a vehicle crossing a simply supported bridge, Journal of Bridge Engineering, 2006; (2) , 241-249.

[3] Fryba, L., *Vibration of Solids and Structures under Moving Loads*, 3rd edition. Thomas Telford Ltd, London, 1999

[4] Hallquist, J. O., *LS-DYNA Keyword User's Manual Volume I*, Livermore Software Technology Corporation (LSTC), Livermore, CA, 2013

[5] Kwasniewski, L.; Wekezer, J.; Roufa, G., Li, H.; Ducher, J.; Malachowski, J., Experimental evaluation of dynamic effects for a selected highway bridge, Journal of Performance of Constructed Facilities, 2006a; 20(3) , 253-260
[6] Kwasniewski, L.; Li, H.; Wekezer, J.; Malachowski, J., Finite-element analysis of vehicle-bridge interaction, Finite Elements in Analysis and Design, 2006b; 42(11) , 950-959
[7] Kwasniewski, L., Nonlinear dynamic simulations of progressive collapse for a multistory building, Engineering Structures, 2010; 32, 1223-1235
[8] Li, H.; Wekezer, J.; Kwasniewski, L., Dynamic response of highway bridge subjected to moving vehicles. Journal of Bridge Engineering, 2008; 13(5) , 439-448.
[9] Olsson, M., Finite element, modal co-ordinate analysis of structures subjected to moving loads, Journal of Sound and Vibration, 1985; 99(1) , 1-12